



HAL
open science

Organic matter deposition in the Ghadames Basin (Libya) during the Late Devonian-A multidisciplinary approach

Armelle Riboulleau, Amalia Spina, Marco Vecoli, Laurent Riquier, Melesio Quijada, Nicolas Tribovillard, Olivier Averbuch

► To cite this version:

Armelle Riboulleau, Amalia Spina, Marco Vecoli, Laurent Riquier, Melesio Quijada, et al.. Organic matter deposition in the Ghadames Basin (Libya) during the Late Devonian-A multidisciplinary approach. *Palaeogeography, Palaeoclimatology, Palaeoecology*, 2018, 497, pp.37-51. <10.1016/j.palaeo.2018.02.004>. <hal-01780055>

HAL Id: hal-01780055

<https://hal.sorbonne-universite.fr/hal-01780055v1>

Submitted on 27 Apr 2018

HAL is a multi-disciplinary open access archive for the deposit and dissemination of scientific research documents, whether they are published or not. The documents may come from teaching and research institutions in France or abroad, or from public or private research centers.

L'archive ouverte pluridisciplinaire **HAL**, est destinée au dépôt et à la diffusion de documents scientifiques de niveau recherche, publiés ou non, émanant des établissements d'enseignement et de recherche français ou étrangers, des laboratoires publics ou privés.



HAL Authorization

1 **Organic matter deposition in the Ghadames Basin (Libya) during the Late Devonian—a**
2 **multidisciplinary approach**

3
4 ¹ Armelle Riboulleau *

5 ² Amalia Spina

6 ³ Marco Vecoli¹

7 ⁴ Laurent Riquier

8 ¹ Melesio Quijada

9 ¹ Nicolas Tribouvillard

10 ¹ Olivier Averbuch

11
12 ¹ Laboratoire d'Océanologie et de Géosciences, UMR 8187, Université de Lille, CNRS,
13 Université du Littoral Côte d'Opale, 59655 Villeneuve d'Ascq, France.

14 ² Department of Physics and Geology, University of Perugia, Perugia, Italy

15 ³ Evolution, Ecologie et Paléontologie - UMR CNRS 8198, Université de Lille, 59655
16 Villeneuve d'Ascq, France

17 ⁴ Sorbonne Universités, UPMC Univ. Paris 06, CNRS, UMR IStEP, 75252 Paris, France

18
19 * corresponding author:

20 e-mail address: armelle.riboulleau@univ-lille1.fr (Armelle Riboulleau)

21
22
23 **Abstract**

24 The organic rich deposits of Late Devonian age are the second most important
25 petroleum source rocks in the Ghadames Basin (Libya). From available stratigraphy, the peak
26 of organic matter deposition, corresponding to a level of radioactive shales easily recognized
27 in gamma ray logs, occurred at the Frasnian-Famennian transition. The present study was
28 focused on samples from borehole D1-26, located in the central part of the Ghadames Basin,
29 belonging to the Aouinet Ouenine III and IV formations (Frasnian to Famennian). The
30 mineral and organic content of the rocks were analyzed in order to determine the origin of
31 organic matter accumulation and estimate if the organic matter enrichment could be related to

¹ Present address: Biostratigraphy Group, Exploration Technical Services Department, Saudi
Aramco, Dhahran, Saudi Arabia

32 the well-known Upper Kellwasser event. The results indicate that during the Frasnian, the
33 planktonic primary productivity was moderate, but anoxic conditions reaching the euphotic
34 zone were frequent and allowed efficient preservation of the organic matter. At the Frasnian-
35 Famennian transition, the deposition of the radioactive shales level can be related to a eustatic
36 rise, which allowed incursion of nutrient-rich water in the basin, leading to increase in
37 primary productivity and photic zone anoxia. During the Famennian, the conditions changed,
38 associated with a relative sea level fall and/or a progradation of detrital sediments originating
39 from the south. Photic zone anoxia was only episodic and plankton-derived organic matter
40 was poorly preserved. Nevertheless, the important influx of organic matter of terrestrial origin
41 allowed significant enrichment of the sediment in organic matter. Several indications suggest
42 the radioactive shales interval could be coeval with the Upper Kellwasser level, nevertheless
43 further stratigraphic work is needed to confirm this hypothesis.

44

45 **Keywords**

46 Biomarkers, palynofacies, major and trace elements, Frasnian-Famennian

47

48 **1. Introduction**

49 The Late Devonian was a period of extensive organic matter (OM) deposition along
50 continental margins (Ulmishek and Klemme, 1990). The reasons for such widespread
51 deposition of OM within oceanic realm is still a matter of discussion but a combination of
52 several favorable factors has been proposed, including: (1) an overall rise of the sea level and
53 a warmer climate favoring water stratification (Ulmishek and Klemme, 1990; Bond and
54 Wignall, 2008; Riquier et al., 2010); (2) a tectonic context marked by the onset of the
55 Variscan orogeny inducing both an increase of the nutrient supply from continents and the
56 reduction of sea-water communications along the former Paleotethysian seaways
57 (Tribovillard et al., 2004; Averbuch et al., 2005); (3) the development of root systems in
58 terrestrial plants during this interval that may have also contributed to an increase in nutrient
59 delivery to oceanic basins, promoting planktonic productivity (Algeo and Scheckler, 1998).
60 The maximum convergence of these favoring conditions resulted in several anoxic events
61 associated with biotic crises, the most famous of which, called the Kellwasser event, occurred
62 at the Frasnian-Famennian boundary; it is characterized by the widespread deposition of two
63 organic-rich levels respectively called the Lower and Upper Kellwasser levels (Buggisch,
64 1991; Joachimski and Buggisch, 1993; House, 2002; Bond et al., 2004; Racki, 2005; Riquier
65 et al., 2006; Becker et al., 2012). Though considered as one of the major extinction events in

66 Earth history, affecting both marine and continental faunas (see McGhee et al., 2013 for a
67 recent review), the exact timing, causes and consequences of the Kellwasser event is still a
68 matter of active research (Racki, 2005; Becker et al., 2016). The resultant massive organic
69 carbon burial may have had a major impact on the global carbon cycle thereby enhancing a
70 significant drop of the CO₂ atmospheric content and a global cooling trend in Late Devonian
71 times (Algeo et al., 1995; Joachimski and Buggisch, 2002; Godderis and Joachimski, 2004;
72 Averbuch et al., 2005; Riquier et al., 2010).

73 North Africa is characterized by the presence of several large to giant petroleum
74 systems associated with Paleozoic source rocks (Boote et al., 1998; Craig et al., 2008). In well
75 logging, the organic-rich intervals are recognizable by their high radioactivity in gamma ray
76 logs, and are qualified as “radioactive shales” or “hot shales”. The dominant source rocks in
77 North African petroleum systems are of Silurian age, in particular the Tanezzuft Formation in
78 Algeria Tunisia and Libya, which base shows a characteristic hot shales interval (Boote et al.,
79 1998; Craig et al., 2008). Organic-rich deposits of Late Devonian age are also widespread in
80 North Africa and represent the second most important source rocks (Boote et al., 1998;
81 Echikh, 1998; Lüning et al., 2003). From available stratigraphic correlations, the age of the
82 Upper Devonian hot shales nevertheless varies from the early Frasnian to the early
83 Famennian, from one basin to the other (Lüning et al., 2003). In the Ghadames Basin (Libya
84 and Tunisia, Fig. 1), the Upper Devonian organic-rich level corresponds to a radioactive
85 shales and limestones interval of late Frasnian age, sometimes referred to as the Cues
86 limestones Horizon (Massa, 1988; Weyant and Massa, 1991). This interval well recognized in
87 gamma ray logs (Weyant and Massa, 1991; Boote et al., 1998) could therefore be coeval to
88 the Upper Kellwasser horizon (Joachimski and Buggisch, 1993; Bond et al., 2004). The two
89 Kellwasser levels are well known in Morocco (Riquier et al., 2005), and Soua (2014)
90 proposed that the two late Frasnian hot-shale intervals detected in South Tunisia were coeval
91 to the Kellwasser levels.

92 This paper presents the results of a multidisciplinary study of a Frasnian-Famennian
93 section in the Libyan part of the Ghadames Basin. The aim of the study was to determine the
94 factors which favored OM deposition in this basin during the Late Devonian, and potentially
95 relate it to the general context of the extensive Kellwasser environmental crisis.

96

97 2. Materials and methods

98 2.1 Studied interval

99 This study is based on samples from borehole D1-26 (30° 29' 21" N, 10° 46' 28" E)
100 cored in 1960-61 by the Oasis Oil Company in Libya, in the central part of the Ghadames
101 Basin (Fig. 1). Samples were taken from cores 6, 7 and 8 in the Aouinet Ouenine (or Awaynat
102 Wanin) formations III and IV (AO III and AO IV, Fig. 2) and were labeled according to their
103 depth in the core, originally given in feet. In the studied borehole, the AO III and AO IV
104 formations mostly consist in grey to dark grey, finely laminated and micaceous shales to silty
105 shales (Fig. 2). The upper part of the AO III Fm. is more calcareous and passes to alternating
106 shales and fossiliferous limestones in the lower part of the AO IV Fm. (Fig. 2). This latter
107 interval should correspond to the "Cues Limestone Horizon" and associated radioactive shales
108 (Weyant and Massa, 1991). Sandy levels appear and become more abundant in the upper part
109 of the AO IV Fm. (Fig. 2). Biostratigraphic constraints, based on palynomorphs and
110 conodonts, and gamma ray correlations with other cores from the Ghadames Basin (Loboziak
111 and Streel, 1989; Weyant and Massa, 1991; Spina et al., 2017), indicate that the samples from
112 core 8 are of late Frasnian age, likely within the *Palmatolepis rhenana* conodont Zone (Streel,
113 2009), while those from core 6 are of late Famennian age (Fig. 2), likely within the
114 *Siphonodella praesulcata* conodont Zone (Streel, 2009). Core 7 was collected in so-called
115 radioactive shales (Massa, 2005, personal communication). This radioactive shale interval
116 generally is considered of late Frasnian age (Massa, 1988; Boote et al., 1998). Nevertheless,
117 Weyant and Massa (1991) analyzed the conodont content of two samples of unknown depth
118 from core 7, and proposed an early Famennian age, in the Middle to Upper *Palmatolepis*
119 *triangularis* Zone, or *Palmatolepis crepida* Zone.

120

121 2.2 Palynology

122 Eighteen core samples from the Aouinet-Ouenine III and IV formations (samples 7813
123 to 7081, 2381.4 m to 2158.3 m) were processed and analyzed. About 20-30 g of sample have
124 been initially treated in hydrochloric acid (37 %), followed by digestion in hydrofluoric acid
125 (50 %) and by treatment in 30% boiling hydrochloric acid to remove fluorosilicates. Residues
126 were then subjected to density separation using zinc bromide solution in order to separate OM
127 from heavy minerals. Finally, the organic-rich residues were sieved with acid resistant 50 and
128 15 µm sieves. No oxidation by nitric acid was performed. A minimum of three palynological

129 strew-slides were mounted for each sample using Eukitt as mounting medium. Palynological
130 slides were examined using transmitted light microscopes, commonly with $\times 20$ (dry) and
131 $\times 100$ (oil immersion) objectives. Palynological slides are stored in the collection of the UMR
132 8198 Evo-Eco-Paleo, Université de Lille-CNRS, Villeneuve d'Ascq (France). For
133 palynofacies analysis, 300 particles were counted in each level, in order to estimate the
134 proportions of the organic constituents. The organic constituents from D1-26 borehole were
135 grouped according to Whitaker (1984) classification, modified to emphasize the organic
136 components useful for palaeoenvironmental observations in the Devonian time span. The
137 allochthonous fraction, of continental origin, includes the palynomaceral group (plant debris)
138 and sporomorphs. The palynomaceral (PM) group is divided in PM1, orange to dark brown
139 fragments, translucent, partially oxidized; PM2, cell-structured orange to dark-brown
140 fragments, moderately oxidized; PM4, black opaque fragments, strongly oxidized. PM4 is the
141 most stable palynomaceral and can be transported for a long distance before being degraded.
142 Sporomorphs mostly correspond to cryptospores (Strother, 1991) and miospores (Steemans,
143 1999). The autochthonous fraction, of marine origin, comprises acritarchs, prasynophycean
144 cysts, chitinozoans and amorphous organic matter (AOM). Acritarchs are organic-walled
145 microfossils of uncertain biological affinity (Evitt, 1963), but mostly representing marine
146 phytoplankton (Tappan, 1980; Martin, 1993; Colbath and Grenfell, 1995). In the Aouinet
147 Ouenine sediments, prasynophycean cysts mainly correspond to *Tasmanites* (Tasmanaceae).
148 This type of algal microfossil occurs in many marine facies from Cambrian to Miocene
149 (Martín-Closas, 2003). Abundance of *Tasmanites* is often observed in marine (shelf and
150 oceanic) organic-rich sediments (Tyson, 1995). Chitinozoans are organic-walled microfossil
151 of uncertain affinity, but most probably representing marine microzooplankton (Paris and
152 Nölvak, 1999). AOM is the degradation product of benthic and pelagic cyanobacteria and
153 sulfur bacteria in oxygen deficient environments. Being the most dissolvable OM, it can be
154 preserved only in oxygen-deprived (suboxic to anoxic) environments, where it is not
155 destroyed and biodegraded by consumers and decomposers or by the oxidizing processes
156 (Hart, 1986). The quantity of this latter was established on unfiltered palynological residues,
157 counting only particles larger than 50 μm .

158

159 2.3 Bulk geochemistry

160 Twelve samples in the 2158.3 m to 2381.4 m interval (samples 7081 to 7813) were
161 analyzed for bulk geochemistry. Rock-Eval analyses were performed on 100 mg of ground

162 bulk rock at the Institut Français du Pétrole-Energies Nouvelles using a Rock-Eval 6
163 apparatus and standard analytical conditions (Behar et al., 2001). The main parameters
164 obtained are total organic carbon content (TOC, in weight %), Hydrogen index (HI, mg HC/g
165 TOC), oxygen index (OI, mg CO₂/g TOC), that are proportional to the H/C and O/C ratio of
166 the kerogen, respectively, and Tmax, an indicator of OM maturity. The sulfur content was
167 determined by elemental analysis of the sediment with a FlashEA 1112 Elemental Analyser
168 (Thermo). The analysis was performed on 1.5 to 2 mg of ground bulk rock added to
169 approximately 5 mg of vanadium pentoxide, used as a combustion catalyst. 2.5-Bis(5-tert-
170 butyl-benzoxazol-2-yl)thiophene (BBOT) was used as standard.

171 Major, minor, trace and rare earth elements (REE) concentrations were determined on
172 ground bulk rock by inductively coupled plasma optical emission spectrometry (ICP-OES)
173 and inductively coupled plasma mass spectrometry (ICP-MS), at Activation Laboratories Ltd.
174 (Ancaster, Canada). Samples were mixed with a flux of lithium metaborate (LiBO₂) and
175 lithium tetraborate (Li₂B₄O₇), and fused in an induction furnace. Molten sample was
176 immediately poured into a solution of 5% nitric acid (HNO₃) containing an internal standard,
177 and mixed continuously until completely dissolved. The analytical accuracy and precision are
178 found to be better than 1–2% for major elements, 5% for REE and 5–10% for the other
179 elements, as checked by international standards and analysis of replicate samples. The
180 enrichment factors were calculated for trace elements often enriched biogenically or
181 authigenically, as follows: $X_{EF} = [(X/Al)_{\text{sample}} / (X/Al)_{\text{PAAS}}]$, where X and Al represent the
182 weight % concentrations of element X and Al, respectively. Samples were normalized using
183 the Post Archean Average shale (PAAS) compositions (McLennan, 1989). An enrichment
184 factor larger than 1 theoretically points to the enrichment of the element relative to the PAAS
185 ; in other words it indicates whether an element is biogenically or authigenically enriched
186 compared to what its concentration would be, if it were of merely clastic origin. Practically,
187 enrichment factors are taken into consideration when they out pass the value of 3. Full results
188 are provided in Table S1. For calculation purpose, concentrations below the detection limit
189 (Table S1) were taken as half the value of the detection limit.

190

191 2.4 Biomarker analysis

192 For biomarker analysis, rock fragments were extracted (24 h) with dichloromethane
193 (DCM) in a refrigerator to remove possible contamination from the sample surface. The
194 fragments were then crushed to extract the lipids from inside the rock. Ca. 30 g pulverized

195 sample were extracted using a soxhlet apparatus with DCM (24 h). Elemental sulfur was
196 removed by addition of activated copper to the recovered extracts. The solvent was removed
197 by means of rotary evaporation and the residue re-dissolved in cyclohexane. The
198 cyclohexane-soluble fraction (maltenes) was further separated by means of column
199 chromatography. A mixture of standard compounds (2,2,4,4,6,8,8-heptamethylnonane, Dr
200 Ehrenstorfer-GmbH; anthracene D10, Dr Ehrenstorfer-GmbH; nonadecan-2-one, Sigma-
201 Aldrich) was added to the maltenes prior to fractionation. The aliphatic fraction was
202 recovered from the maltenes by elution with cyclohexane on an activated silica column.
203 Elution with a mixture of cyclohexane/DCM (9/1, v/v) recovered the aromatic fraction, after
204 which the polar fraction was recovered by elution with DCM/MeOH (1/1, v/v). The aliphatic
205 and aromatic fractions were analyzed by way of gas chromatography-mass spectrometry
206 (GC-MS) using either a Trace GC 2000 gas chromatograph equipped with a DB5ht column
207 (30 m × 0.25 mm i.d.; 0.1 μm film thickness). The oven temperature program was: 100 °C (1
208 min) to 310 °C (held 16.5 min) at 4 °C/min. Helium was used as carrier gas. The mass
209 spectrometer conditions were as follow: ionization energy 70 eV for electron ionization (EI)
210 with a mass range m/z 50–700. Alternatively, samples were analyzed with a Perkin Elmer
211 Clarus 680 GC equipped with a DB5MS ultra inert column (30 m × 0.25 mm i.d.; 0.25 μm
212 film thickness). The oven temperature program was: 60 °C (1 min) to 100°C at 15°C/min,
213 from 100°C to 200°C at 3°C/min, from 200 °C to 310 °C (held 20 min) at 4 °C/min. Helium
214 was used as carrier gas. The mass spectrometer was operated at 70 eV for electron ionization
215 (EI) with a mass range m/z 50–550 (full scan). Compounds were identified by comparison of
216 mass spectra and elution order with published data.

217

218 **3. Results and interpretation**

219 **3.1 Palynofacies**

220 The palynofacies of the studied samples shows variable proportions of palynomorphs as well
221 as AOM (Fig. 3). The palynofacies of the first levels from the AO III Fm. (base of core 8,
222 samples 7813 to 7809, Fig. 3) shows high abundances of acritarchs and prasinophycaean
223 cysts (tasmanaceans) representing about 40% of the entire palynofacies. AOM is abundantly
224 present in this interval, reaching up to ~40% of the palynofacies. Partially oxidized
225 palynomacerals (e.g. PM1+PM2) and sporomorphs are scarcely present. Chitinozoans are
226 relatively abundant (5-7 %). In the overlying levels of the AO III Fm. (samples 7802 to 7780,

227 Fig. 3), the palynofacies is dominated by the same marine elements but the proportion of
228 acritarchs and tasmanaceans increases (up to 60 %) while the AOM content is reduced (0 to
229 10 %). At the base of AO IV Fm. (core 7, Fig.3), corresponding to the "radioactive shales",
230 AOM in high proportion, acritarchs and prasynophycean cysts characterize almost all the
231 entire palynofacies. Sporomorphs and chitinozoans are very rare to absent. The acritarch
232 fauna is well diversified in the samples from cores 8 and 7. A distinctive change in the
233 palynofacies composition marks the uppermost levels (core 6) of AO IV Fm. (samples 7100
234 to 7081, Fig. 3). Strongly oxidized palynomacerals (PM4) and partially oxidized
235 palynomacerals (PM1 + PM2) are abundant as well as well-preserved sporomorphs. This
236 latter group reaches abundance around 35% in the levels close to the boundary with the
237 overlying Tahara Fm. Microplankton here mainly consists of acritarchs (10 to 15 %).
238 *Tasmanites* are uncommon (≤ 10 %). AOM and chitinozoans are very rare or absent.
239

240 3.2 Bulk geochemistry

241 3.2.1 Organic matter and sulfur

242 Total organic carbon (TOC) contents of the analyzed samples vary between 0.8 and
243 2.8 % (average 1.75 %, Table 1). Tmax values range between 431 and 440 °C. Average Tmax
244 value in the uppermost samples is 435 °C indicating the beginning of the oil window. The
245 average Tmax value is slightly higher in the samples from core 8 (438 °C) indicating a
246 slightly higher thermal maturity.

247 HI values are between 60 and 319 mg HC/g TOC (av. 132 mg HC/g TOC) while OI
248 values range between 0 and 47 mg CO₂/g TOC. In a pseudo van Krevelen (HI-OI) as well as
249 in the HI-Tmax diagram (Fig. 4A), the samples plot in the area of Type II-III OM. TOC/N
250 atomic ratios vary between 14 and 44 (Table 1). In average, higher values are observed in the
251 samples from core 6 (av. 38) than in samples from cores 7 and 8 (av. 18). Higher values of the
252 C/N ratio in the samples from the top of AO IV Fm. (samples 7100 to 7081) suggest a higher
253 contribution from woody organic matter (Meyers, 1997), which is consistent with
254 palynofacies observations.

255 The sulfur content of the sediment is relatively high, with an average value of 2.8 %.
256 In a S vs TOC plot (Fig. 4B), most samples plot above the "normal marine" line (Berner,
257 1982), having a slope of 2 for the Devonian (Berner and Raiswell, 1983). It can be argued that
258 this feature could result from a TOC loss upon maturation and petroleum expulsion, since

259 Rock Eval production index (PI) values between 0.10 and 0.48 are compatible with oil
260 expulsion (Table 1). Nevertheless, considering an initially doubled TOC values does not
261 significantly change the S-TOC relationship as most samples would remain above this
262 “normal marine” line (Fig. 4C). This S-TOC behavior is often considered as indicating
263 deposition under strongly reducing to euxinic conditions (Leventhal, 1983).

264

265 3.2.2 Productivity (Ba, Ni, Cu) and redox proxies (Mo, U, V, Ni, Cu, Zn, Co, Cr, Ce*)

266 In order to be valid as productivity or redox proxies, elements must not be positively
267 correlated with the Si (quartz) and/or Al (clay) content of the sediment. In the studied
268 samples, Si and Al are negatively correlated, suggesting that the clay and silica content vary
269 in opposite proportions. Most productivity and redox-sensitive elements in D1-26 samples are
270 neither correlated with Si nor Al, except for Cr which is positively correlated with Al ($r =$
271 0.818 , $n=12$) and Ba which is positively correlated with Si ($r = 0.933$, $n=12$). The latter
272 correlation might indicate the presence of silica of biogenic origin. The average value of the
273 Ge/Si ratio of $8.1 \cdot 10^{-6}$ however points for a mainly detrital origin of the silica in D1-26
274 samples, therefore corresponding to detrital quartz (Tribouillard, 2013). This indicates that Cr
275 and Ba have a dominant detrital origin and cannot be considered as environmental proxies.

276 The average enrichment factors (EF) of the different elements which are not
277 influenced by the detrital supply range between 0.5 and 3 (Fig. 5A), pointing for no
278 significant authigenic enrichment in these sediments. In detail, most elements do not show a
279 marked temporal trend except for molybdenum. The Mo_{EF} curve shows values generally
280 above 1 in the lowermost samples and a maximum value (22) in sample 7712. Above this
281 sample, Mo is below the detection limit (Table S1) so that Mo_{EF} values are below 1. The
282 cerium anomaly (Ce*), though potentially influenced by changes in the detrital flux and sea
283 level variations (Wilde et al., 1996), is negative for all the samples (average -0.048). The
284 temporal variations of Ce* are somehow opposite to Mo variations, the lowest values being
285 observed in the lowermost samples, while higher values are observed in the upper part of the
286 studied interval (Fig. 5B). Overall, these data point for only moderately reducing conditions
287 during deposition of the two formations. The most reducing conditions, as indicated by the
288 highest enrichment in molybdenum, are observed in the sample 7712, corresponding to the
289 base of the organic-rich, radioactive clays. The AO III Fm. overall appears deposited in
290 slightly more reducing conditions than the AO IV Fm.

291

292 3.2.3 Detrital proxies

293 In addition to Si and Al, elements mostly associated with detrital minerals comprise K
294 (feldspar and/or illitic clay minerals), Ti (rutile, titanite or ilmenite), Zr (zircon) and rare earth
295 elements (REE, which can be associated with several heavy minerals; Mongelli, 1995; Cullers
296 and Podkovyrov, 2002). When normalized to the Al content, the concentration of these
297 elements is a good indicator of changes in the detrital flux.

298 The geochemical composition of the lowermost five samples is relatively constant
299 (Fig. 6). Only REE ratios show slight variations in this part (Fig. 6B). From sample 7780
300 upwards the geochemical composition is more variable, with overall higher element/Al ratios
301 for Ti, Hf, Th and Zr (Fig. 6A). The REE profiles also are more variable as indicated by the
302 (La/Lu)_N and (Gd/Yb)_N ratios (Fig. 6B). For major and trace elements a maximum in the Al-
303 normalized content is observed in the sample 7087 (Fig. 6A). This sample is also
304 characterized by a PAAS-normalized REE pattern markedly different from that of the other
305 samples (Fig. 7).

306 Increase and variability of Al-normalized concentration of the different elements
307 considered here mainly indicate a change from an argillaceous AO III Fm. to a more silty or
308 more sandy AO IV Fm. The relative stability of REE patterns in the studied samples —except
309 for sample 7087— suggests that these changes are mainly due to grain sorting rather than
310 from changes in the origin of the detrital grains. In the case of sample 7087, the REE pattern
311 of which is markedly different, the higher Zr/Al and Hf/Al ratios indicate a higher proportion
312 of heavy minerals in the sediment. Such characteristics are observed in sediments deposited
313 by turbidity currents (e.g. Riboulleau et al., 2014) and can be related to the increased
314 proportion of sandy layers in the upper part of the AO IV Fm., reflecting a relative sea-level
315 fall during the deposition of this formation (Massa, 1988; Carr, 2002).

316

317 3.3 Biomarkers

318 3.3.1 Saturated fraction

319 The saturate fraction is dominated by a series of linear alkanes (*n*-alkanes). Hopanes,
320 steranes, linear isoprenoids and cycloalkanes are present in lesser proportion.

321 *n*-Alkanes range from C₁₃ to C₃₇ with a maximum in C₁₆ or C₁₇ (Fig. 8A). The
322 contribution from long chain *n*-alkanes is generally low, as indicated by the low value of the
323 terrestrial to aquatic *n*-alkane ratio (TAR; Bourbonniere and Meyers, 1996; TAR values 0.06-

324 0.52). Only the sample 7085 shows a higher contribution of long-chain alkanes (TAR = 0.74).
325 No marked even or odd predominance is observed, as indicated by the CPI values close to 1
326 (Bray and Evans, 1961). The highest CPI values (1.2) are observed in the two uppermost
327 samples (7087 and 7085). Linear isoprenoids range from C₁₄ to C₂₃, maximum in C₁₉. The
328 Pr/Ph ratio ranges from 1.0 to 2.2. This highest value is obtained for the two uppermost
329 samples.

330 The distribution of bicyclic and tricyclic terpenoids is similar in all the samples.
331 Bicyclic sesquiterpenoids range from C₁₄ to C₁₆ and are dominated by *ent*-8β(H)-
332 homodrimane followed by a C₁₅ compound (Fig. 8B). *Ent*-8β(H)- drimane is also present in
333 lesser amount. Three C₁₉ tricyclic terpanes are also present in low abundance in all the
334 samples. From its mass spectrum, the first eluting compound corresponds to a 13α(methyl)-
335 tricyclic terpane previously as described by Wang and Simoneit (1995). No other element
336 from this series is apparently present. The following compounds correspond to compounds B
337 and C of Greenwood and George (1999). A series of regular tricyclic terpanes (cheilantanes)
338 ranging from C₁₉ to C₂₆ (max C₂₃) is also observed in all the samples (Fig. 8C).

339 Hopanoids are present in all the samples but are relatively more abundant in the two
340 uppermost samples. Hopanoids are dominated by a series of C₂₇ to C₃₄ regular αβ hopanes
341 (Fig. 8C). βα Moretanes ranging from C₂₉ to C₃₄ are present in low abundance. In addition,
342 several series of rearranged hopanes are observed: C₂₄ and C₂₆ 17,21-secohopanes (Lu et al.,
343 2009), C₂₉ and C₃₀ 17α(H)-diahopanes, C₂₇ to C₃₀ 18α(H)-neohopanes (Ts series) and C₂₉-C₃₂
344 early eluting series (Moldowan et al., 1991; Farrimond and Telnæs, 1996). Norgammacerane
345 and gammacerane are also detected in low amounts, mostly in the two uppermost samples.

346 Steroids are present in all the samples, but in very low abundance. They are slightly
347 more abundant in the two uppermost samples. The distribution of compounds is comparable
348 in all the samples with a few variations, and comprises the dia- and regular series, dominated
349 by the C₂₇ and C₂₉ compounds (Fig. 8D, Table 2). Diasteroids are relatively less abundant in
350 the two uppermost samples (Table 2). Methylsteranes and dinosterane isomers were not
351 detected. Short chain steroids C₂₁ to C₂₃ are also observed in all the samples (Fig. 8D). They
352 are generally present in relatively low abundance compared to the longer C₂₇-C₂₉ compounds.
353

354 3.3.2 Aromatic fraction

355 This fraction is dominated by polycyclic aromatic hydrocarbons (PAHs) among which
356 naphthalenes and phenanthrenes. Aromatic biomarkers mostly correspond to triaromatic
357 steroids and arylisoprenoids.

358 Triaromatic steroids are observed in all the samples (not shown). They range from C_{20}
359 to C_{28} and are dominated by the C_{26} to C_{28} compounds. Short chain compounds (C_{20} - C_{22}) are
360 however more abundant in the lower samples. The distribution is dominated by the C_{28}
361 compounds for all the samples, however, the uppermost 2 samples show a higher contribution
362 of the C_{26} compounds. 3-Methyl and 4-methyltriaromatic steroids are also present in minor
363 proportion in all the samples, however no triaromatic dinosteroids were identified.

364 Aromatic compounds derived from hopanoids were detected in very low proportions
365 in the two uppermost samples. They mostly correspond to a C_{24} ABCD-tetraaromatic
366 hopanoid and des-E-D:C-friedo-25-norhopa-5,7,9-triene identified by Hauke et al. (1993).
367 Cadalene is present in trace amounts in all the samples. Retene and the aromatic abietanoids
368 were not detected.

369 A series of 2,3,6-trimethyl-arylisoprenoids ranging from C_{13} to C_{31} (max C_{18}) is
370 observed in all the samples (Fig. 9). This series of compounds is well known as the product of
371 degradation of isorenieratene (Requejo et al., 1992). A second series corresponding to 3,4,5-
372 trimethyl-arylisoprenoids is also observed (Fig. 9). These compounds derived from the
373 degradation of the aromatic carotenoid palaerenieratene (Brown et al., 2000) are present in all
374 the samples except the two uppermost samples (7087 and 7085). Isorenieratane was detected
375 in low amount in all the samples while palaerenieratane is observed in the four lowest
376 samples (7812 to 7712). Several other diagenetic/catagenetic products of isorenieratene
377 previously described by Koopmans et al. (1996) were also detected in all the samples, where
378 they show a similar distribution: a series of diaromatic isoprenoids with a biphenyl head
379 characterized by a m/z 237 fragment ranging from C_{19} (max) to C_{22} , and C_{21} to C_{24} diaromatic
380 compounds characterized by a m/z 133 fragment (compounds I to III, Fig. 9).

381 Alkylated di-, tri-, tetra-, and pentaaromatics are detected in abundance in all the
382 samples. Naphtalene and methylated counterparts from C_1 to C_6 are present in all the samples.
383 They are dominated by the C_2 or C_3 isomers. Phenanthrenes from C_0 to C_4 are observed in all
384 the samples. Phenanthrene is the most abundant compound. Dibenzofurans are present in all
385 the samples, but their proportion is higher in the uppermost two samples. They range from C_0
386 to C_2 and are dominated by the C_1 isomers. Dibenzothiophenes (DBT) from C_0 to C_3 are
387 observed in all the samples. Their relative abundance is however lower in the two uppermost

388 samples. Their distribution is dominated by DBT or by 4-methyl-DBT. Fluoranthene, pyrene
389 and methylated counterparts from C₁ to C₂ are detected in all the samples, however, their
390 relative abundance is higher in the two uppermost samples. Triphenylene, chrysene their
391 methylated counterparts from C₁ to C₄ are present in all the samples. The relative abundance
392 of the C₀ counterparts and relative distribution of methylated homologs however differs
393 between the lower four and upper two samples. In particular, a large dominance of the non-
394 methylated counterparts is observed in the two uppermost samples. Isomer distribution ratios
395 of selected PAHs are presented in Table 2.

396 Highly condensed PAH's such as benzo[e]pyrene, benzo[ghi]perylene or coronene are
397 observed only in the uppermost two samples. They are not observed in the lowermost four
398 samples, even by selective ion detection.

399

400 **4 Discussion**

401 4.1 Organic matter maturity

402 From the Rock-Eval Tmax values (Fig. 4A), the studied samples are located at the
403 beginning of the oil window, with slightly higher maturity for samples from core 8 than for
404 samples from core 6. This range of maturity is also indicated by the color and state of
405 preservation of the miospores, acritarchs and *Tasmanites* in the samples (Spina et al., 2017).
406 Using average correlation between biomarker isomerization ratios and thermal maturity
407 (Peters et al., 2005), the ratio obtained in the studied samples (Table 2) tends to indicate a
408 higher maturity than Rock-Eval Tmax, samples from core 8 having reached the peak of oil
409 generation while samples from core 6 would be slightly less mature. Methylphenanthrene
410 isomerization ratios indicate even more maturity with calculated vitrinite reflectance values
411 higher than 0.7 % (Table 2). Hrouda (2004) previously observed a relatively poor correlation
412 between molecular maturity indicators, vitrinite reflectance and Rock Eval in the Upper
413 Devonian formations of the Ghadames Basin. Nevertheless, the relatively low maturity
414 indicated by the Rock Eval data is supported by vitrinite reflectance measurements of 0.51 to
415 0.59 performed by Underdown et al. (2007) on the same depth interval. These maturities are
416 also consistent with those obtained by Hrouda (2004) for Upper Devonian formations in
417 nearby cores from the Ghadames Basin. This low maturity allows interpret further the
418 biomarker distribution in the analyzed samples.

419

420 4.2 Organic matter source

421 Based on palynofacies analysis, TOC/N ratio, and biomarker content, the OM in the
422 Aouinet Ouenine Fm. shows a mixed contribution from continental and marine fractions. The
423 palynofacies content and TOC/N ratio allow to clearly distinguish the lower samples (AO III
424 Fm. and radioactive shales) dominated by marine elements from the upper part of AO IV Fm.,
425 where the contribution from continental OM is more significant. Such distinction is less
426 obvious basing on the biomarkers, since terrestrial plant biomarkers are almost absent from
427 the record. Terrestrial plants in the Late Devonian were mostly restricted to bryophytes and
428 early tracheophytes (Taylor et al., 2009). Earliest plants have not been so far related to an
429 abundance of diversified biomarkers (Versteegh and Riboulleau, 2010), nevertheless a few
430 higher plant terpenoids were previously identified in Devonian rocks, including in sediments
431 of the Ghadames Basin (Kashirtsev et al., 2010; Romero-Sarmiento et al., 2011). Devonian
432 plants already possessed a waxy coating made of long chain *n*-alkanes, typical of plant
433 cuticles (Eglinton and Hamilton, 1967; Versteegh and Riboulleau, 2010). The dominance of
434 short chain *n*-alkanes (<C₂₀) in the samples is typical of sedimentary OM dominated by an
435 autochthonous algal input (Gelpi et al., 1970). Nevertheless, the increased proportion of long
436 *n*-alkanes in samples from core 6, as indicated by the higher TAR values (Table 2), is
437 consistent with an increased contribution of OM of terrestrial origin. Contribution from land-
438 derived OM in the two samples from core 6 (7087 and 7085) is also indicated by the PAH
439 distribution, showing a high proportion of dibenzofurans, which have been related to
440 dehydration of plant cellulose and polysaccharides (Sephton et al., 1999) and the contribution
441 of unsubstituted highly condensed PAH such as coronene, which have been related to
442 wildfires (Marynowski and Simoneit, 2009).

443 The sterane distribution, dominated by the C₂₉ and C₂₇ isomer (Table 2), is typical of
444 OM of marine origin. Methylated counterparts, in particular 4-methyl isomers are generally of
445 algal origin. Dinosteroids and 4-methyl steroids are often assigned to dinoflagellates and/or
446 acritarchs. Though dinosteroids are absent from the extracts of D1-26 samples, the methylated
447 steroids can be related to the marine algal input. In particular, several studies of Paleozoic
448 rocks and petroleum have related these compounds to acritarchs (Moldowan et al., 1996;
449 Moldowan and Talyzina, 1998).

450 Hopanoids and their diagenesis products, as well as drimane and homodrimane are
451 related to bacterial inputs (Ourisson et al., 1979; Alexander et al., 1983). The sterane/hopane
452 ratio is often used as an indicator of the proportion of bacterial biomass compared to the
453 eukaryotic one. The highest values of this ratio are observed in the samples from the AO IV

454 Fm. and therefore suggest higher contribution from eukaryotes in these samples, while a
455 higher contribution from bacterial biomass is observed in the lowermost four samples.

456 Though their origin is still debated, tricyclic terpanes (cheilantanes) have been mostly
457 related to the contribution from prasinophytes and in particular tasmanaceans (Aquino Neto et
458 al., 1992; Dutta et al., 2006). This is consistent with the frequent observation of *Tasmanites* in
459 the palynofacies of D1-26 samples (Fig. 3). High relative abundances of cheilantanes,
460 indicated by the tricyclic/17 α hopane ratio are observed in the four lower samples (7812 to
461 7712, Table 2). The upper two samples (7087 and 7085) show lower relative abundance of
462 cheilantanes (Table 2), which can be related to the lower relative abundance of *Tasmanites* in
463 the palynofacies (Fig. 3). Abundance of prasinophytes in general or of *Tasmanites* in
464 particular, has also been related to an increase of the C₂₈/C₂₉ sterane ratio (Schwark and Empt,
465 2006). This is for instance the case at the Frasnian-Famennian transition in the famous
466 Kowala section in Poland, where prasinophytes represent 80 to 90% of palynomorphs
467 (Filipiak, 2002; Schwark and Empt, 2006). No relationship is observed between the C₂₈/C₂₉
468 sterane ratio and the relative abundance of *Tasmanites* in the palynofacies of D1-26 samples
469 (Table 2, Fig. 3), which could be related to the fact that prasinophytes rarely account for more
470 than 40% of palynomorphs in these samples.

471

472 4.3 Redox conditions

473 Isorenieratene is a pigment synthesized by green sulfur bacteria (*Chlorobiaceae*),
474 obligate anaerobes requiring light and free sulfides for living (Liaaen-Jensen, 1978;
475 Overmann, 2008). In particular, *Chlorobiaceae* have been observed in the water column of
476 the Black Sea (Overmann et al., 1992). For this reason, the observation of isorenieratene
477 derivatives in sediment extracts is often used as an indicator of photic zone anoxia (Summons
478 and Powell, 1986). The source of palaerenieratene is unknown but several arguments suggest
479 this compound originates from extinct organisms related to *Chlorobiaceae* (Hartgers et al.,
480 1994). A recent review of the occurrence of palaerenieratene in oils and sediments confirms
481 this compound is almost restricted to the Paleozoic (French et al., 2015). When present,
482 palaerenieratene is often more abundant than isorenieratene (Requejo et al., 1992; Behrens et
483 al., 1998; Clifford et al., 1998; Joachimski et al., 2001; Armstrong et al., 2009; Bushnev,
484 2009; Maslen et al., 2009; Racka et al., 2010; Marynowski et al., 2012; Melendez et al., 2013;
485 Tulipani et al., 2015). Changes in the proportion of palaerenieratene vs. isorenieratene
486 derivatives in relation to paleoenvironments are rarely reported in the literature. Nevertheless,
487 in the Middle Devonian Keg River Fm., Behrens et al. (1998) observed that while both

488 palaerenieratane and isorenieratane and their derivatives were present in transgressive facies,
489 the regressive facies of this formation only showed the presence of isorenieratane and its
490 derivatives.

491 The total concentration of isorenieratene and palaerenieratene derivatives in the
492 extracts of D1-26 generally decreases up-section through the studied interval, with the
493 maximum value observed in the lowermost sample and the minimum value in the uppermost
494 sample (Fig. 10A). When plotted in the Pr/Ph ratio versus the aryl isoprenoid ratio (AIR*)
495 modified from Schwark and Frimmel (2004), the lowermost four samples from D1-26 plot in
496 a sector of relatively persistent photic-zone anoxia and reducing sediment, while the
497 uppermost two plot in an area of oxygenated sediment with more episodic photic-zone anoxia
498 (Fig. 10C). Location of D1-26 samples in this plot are also consistent with previous
499 observations in the Posidonia black shale, regarding relative sea-level variations (Schwark
500 and Frimmel, 2004): samples from AO III Fm. and radioactive shales, deposited in a rising
501 sea level plot in the “intermediate sea level” sector, while samples from the higher part of AO
502 IV Fm., deposited in a regressive context, plot in the “high sea level” and “low sea level”
503 sectors. The ratio of the 3,4,5-trimethyl- to 2,3,6-trimethyl-aryl isoprenoids (palaerenieratene
504 to isorenieratene derivatives ratio, PIR) slightly increases from the base to the middle part of
505 the series and falls to 0 in the uppermost two samples (Fig. 10B). The disappearance of
506 palaerenieratane and its derivatives in the regressive, highest part of AO IV Fm. is consistent
507 with the previous observations of Behrens et al. (1998).

508 The abundance of prasinophytes in the palynofacies of D1-26 samples shows a good
509 parallel with the relative abundance of isorenieratene and palaerenieratene and their
510 derivatives in the extracts (Figs. 3, 10): present in significant proportion in AO III Fm. and the
511 radioactive shales, they become minor in the upper part of AO IV Fm. This observation fully
512 supports the proposition of Prauss (2007), who suggested that prasinophyte abundance in
513 sediments is controlled by, and therefore is an indicator of, reducing conditions in the photic
514 zone.

515 Based on redox-sensitive trace metal concentration, the studied Devonian sediments
516 from borehole D1-26 appear deposited under mainly oxic conditions. This appears
517 inconsistent with the occurrence of *Chlorobiaceae* biomarkers and of *Tasmanites*, in all the
518 samples. The only sample showing enrichment in redox-sensitive trace metals is sample 7712,
519 belonging to the very base of the radioactive shales. Its enrichment in uranium remains
520 modest (EF = 2) while a more notable enrichment is observed for molybdenum (EF=21). The
521 contrasted enrichments in Mo and U, respectively suggest molybdenum enrichment

522 associated with redox cycling of manganese or iron oxyhydroxides, at the sediment water-
523 interface or within the water column (Algeo and Tribovillard, 2009). It means that the water
524 column would have been regularly oxygenated but the redox-cline would have been lying at
525 short distance beneath the sediment-water interface, thence an anoxic sediment. High
526 enrichment in trace elements in the radioactive shales is reported by Weyant and Massa
527 (1991), nevertheless these authors did not indicate from which boreholes or outcrops these
528 data originated, moreover, no data are available for the rest of the Aouinet Ouenine group.

529 The discrepancy between molecular and inorganic redox proxies could result from a
530 so-called “reservoir effect” (Algeo, 2004; Algeo and Lyons, 2006). When a basin is poorly
531 connected with the open sea, scavenging of molybdenum and other redox-sensitive trace
532 metals by the precipitation of authigenic minerals may overcome the inflow of these elements
533 to the basin. This process results in the progressive depletion of these elements in the water
534 column (Algeo, 2004; Algeo and Lyons, 2006). Sediments deposited below such depleted
535 water column will not be enriched in trace elements, even if they are organic-rich and/or
536 anoxic (Algeo, 2004; Tribovillard et al., 2008). During the Devonian, the North African
537 domain was structured into several basins separated by topographic highs (Lüning et al.,
538 2003; Guiraud et al., 2005; Wendt et al., 2006; Frizon de Lamotte et al., 2013). Poor
539 connections of the bottom part of these basins with the open sea are suggested by the
540 widespread deposition of organic-rich sediments in the various North African basins (Lüning
541 et al., 2003; Wendt et al., 2006). Such configuration might therefore have favored progressive
542 depletion of the water column in trace elements, leading to the poor enrichment observed in
543 the studied samples from borehole D1-26.

544

545 4.4 Organic matter deposition and relationships with the F/F events

546 The studied samples from the Aouinet Ouenine Group where the TOC content was
547 measured do not include the “radioactive shales” and are not very organic rich (Table 1).
548 Nevertheless, the TOC values from 1 to 2% are consistent with previous studies of the
549 Aouinet Ouenine Group in nearby boreholes (Hrouda, 2004).

550 The different methods used here indicate that in the Frasnian AO III Fm., OM mainly
551 originates from an algo-bacterial biomass. The biomarker content and the significant
552 contribution of *Tasmanites* in the palynofacies indicate that conditions in the sediment and
553 water column were frequently reducing (Fig. 11A). The notable proportion of AOM in the
554 palynofacies (Fig. 3) points to efficient OM preservation under reducing conditions. The
555 moderate TOC values of the sediment despite recurrent anoxia, the notable proportion of

556 land-derived OM, and the abundant and well-diversified fauna of acritarchs in the
557 palynofacies, nevertheless suggest that planktonic productivity was moderate (Fig. 11A).
558 Consistent, Massa (1988) indicates that the facies in the AO III Fm. is confined and that the
559 macrofauna are impoverished.

560 The palynofacies content and biomarkers in the radioactive shales from D1-26
561 borehole only moderately differ with those of the AO III Fm., indicating a dominantly algo-
562 bacterial OM and frequently anoxic conditions in the sediment and water column (Fig.
563 11B,C). The high TOC content documented in the radioactive shales (Massa, 1988) is
564 however a major difference with the AO III Fm., which, added to the low proportion of
565 terrestrial OM in the palynofacies, suggests increased planktonic productivity and eutrophic
566 conditions during deposition (Fig. 11B,C). Chitinozoans have been recently shown to be
567 produced by relatively shelfal epiplanktonic organisms (Vandenbroucke et al., 2010). Their
568 decreased abundance in the palynofacies of the radioactive shales compared to AO III Fm. as
569 well as the absence of sporomorphs are consistent with a more pelagic setting, and therefore
570 an increased sea level (Fig. 11B,C).

571 Eutrophication leading to the deposition of the radioactive shales could have resulted
572 from the input of land-derived nutrients in the basin (Algeo et al., 1995; Averbuch et al.,
573 2005), however, the Late Devonian was dominantly a period of subsidence and not of uplift
574 around the Ghadames Basin (Craig et al., 2008). Moreover, though the detrital elements
575 suggest a change in the detrital flux between AO III and AO IV formations (Fig. 6), this
576 change appears to be modest (Fig. 7) and is already observed in sample 7780, several meters
577 below the radioactive shales. The present data therefore do not support an increased supply of
578 land-derived nutrients in the Ghadames Basin. Since depositional conditions were already
579 reducing in the Ghadames Basin during the deposition of AO III Fm. (Fig. 11A), nutrients
580 could either have been recycled from the water-column by more frequent water-column
581 mixing (Murphy et al., 2000), or originate from incursions of nutrient-rich water from the
582 Paleotethys. On the one hand, we do not have arguments regarding more frequent water-
583 column mixing. On the other hand, incursions of water from the open sea were likely favored
584 by the sea level rise, and are supported by the Mo/Al ratio of the samples (Fig. 5). As
585 previously discussed, the redox-sensitive trace elements suggest that the water column of the
586 Ghadames Basin was relatively depleted in dissolved trace metals during deposition of AO III
587 Fm. The enrichment in molybdenum observed in sample 7712 was therefore only possible
588 because of Mo inputs, refuelled by the ingression of « new » sea water into the basin (Algeo,
589 2004; Algeo and Lyons, 2006).

590 The ambiguity on the age of samples from core 7 compels us to consider several
591 scenarios relating the radioactive shales with the Frasnian-Famennian transition events. Massa
592 (1988; pers. comm., 2005) suggested that the radioactive shales were of latest Frasnian age. If
593 so, the radioactive shales of the Ghadames Basin might be equivalent to the Upper Kellwasser
594 level. The two Kellwasser levels are well known in Morocco (Riquier et al., 2005), and the
595 Frasnian radioactive shales have been related to the upper Kellwasser level in the Berkhine
596 area in Algeria (Lüning et al., 2004) and in southern Tunisia (Soua, 2014). The deposition of
597 the upper Kellwasser level and of the radioactive shales from the Ghadames Basin were both
598 related to a Late Frasnian second-order sea-level high-stand (Carr, 2002; Chen and Tucker,
599 2003; Dardour et al., 2004; Bond and Wignall, 2008). The eutrophication and possible
600 development of more reducing conditions during the Upper Kellwasser event could result
601 from the incursion of nutrient-rich and anoxic waters into the Ghadames Basin originating
602 from the Paleotethys (Fig. 11B). This option would give support to the scenarios relating the
603 deposition of the Kellwasser level to widespread oceanic eutrophication and development of
604 anoxia in marginal basins (Joachimski and Buggisch, 1993; Bond et al., 2004; Averbuch et
605 al., 2005; Riquier et al., 2006; Carmichael et al., 2014).

606 Alternately, if the radioactive shales were of early Famennian age (Weyant and Massa,
607 1991), their deposition could be related to the early Famennian sea-level rise documented in
608 several basins (Sandberg et al., 2002; Haq and Schutter, 2008). Though sea-level variations
609 around the Frasnian-Famennian are still a matter of discussion (Bond and Wignall, 2008), this
610 could correspond to T-R cycle IIe of Johnson et al. (1985). Deposition of black shales in
611 basinal settings during the early Famennian have been described in Poland, France, Morocco
612 and Eastern North America (Wendt and Belka, 1991; Bond et al., 2004; Schieber and Lazar,
613 2004; Riquier et al., 2005) and may be related to this sea-level rise. For instance, in the
614 Illinois Basin, the lowermost deposits of Famennian age in the New Albany shales show a
615 more basal facies and more eutrophic conditions than late Frasnian deposits (de la Rue et
616 al., 2007). The radioactive shales would then correspond to a model of « transgressive black
617 shales », where connection with the open sea allows the entrance of nutrient-rich water and
618 eutrophication (Fig. 11C), as observed in the Cariaco Basin (Venezuela) tuned to Quaternary
619 sea-level oscillations (Peterson et al., 2000).

620 In addition to its well known $\delta^{13}\text{C}$ excursion (Joachimski and Buggisch, 1993), recent
621 studies indicate the Upper Kellwasser level could be characterized by molecular signatures:
622 increase of the $\text{C}_{28}/\text{C}_{29}$ sterane ratio (Schwark and Empt, 2006) related to the prominence of
623 prasinophytes and low values of the hopane/sterane ratio, indicating high relative input of

624 eukaryotes (Haddad et al., 2016). The radioactive shales of borehole D1-26 show a slight
625 decrease of the C_{28}/C_{29} sterane ratio compared to the other samples (Table 2). The
626 hopane/sterane ratio is lower in the radioactive shales than in the samples from the AO IV
627 formation (Table 2). Nevertheless, similarly low hopane/sterane ratios are observed in the
628 samples from AO III Fm. (Table 2). None of these parameters therefore allows clarify the
629 ambiguity on the age of samples from core 7.

630 The highest part of AO IV Fm. is characterized by a change in sedimentary facies
631 compared to underlying levels. The proportion of sand increases (Fig. 2, 6), indicating a more
632 proximal depositional setting. This lithological evolution is related to a third- or second-order
633 relative sea-level fall (Carr, 2002; Dardour et al., 2004; Fig. 11D). Consistent, the OM content
634 changes and is dominated by land-derived material (Fig. 3). The lower sea-level and restricted
635 conditions could have favored oligotrophic conditions in the Ghadames Basin (Fig. 11D).
636 Palynofacies and biomarkers point to relatively oxidative conditions in the sediment (Fig.
637 11D), with only episodic photic zone anoxia. Though conditions were less prone to OM
638 preservation, the highest part of the AO IV Fm. shows TOC values comparable to the AO III
639 Fm. OM enrichment in this interval therefore appears to be related to an increased
640 contribution of relatively resistant and less oil-prone terrestrial OM (Fig. 11D).

641

642

643 **5. Conclusions**

644 The multidisciplinary analysis of the Frasnian-Famennian Aouinet Ouenine III and IV
645 formations in borehole D1-26, located in the Ghadames Basin (Libya) allowed to better
646 understand the factors of OM enrichment in this important petroleum system. Our data
647 indicate that during the Late Frasnian the Ghadames Basin was restricted and subject to
648 frequent episodes of photic-zone anoxia. These conditions allowed a good preservation of
649 OM derived from a moderate phytoplanktonic productivity. The beginning of OA IV Fm. is
650 marked by the deposition of a radioactive shale interval, well known in core loggings of the
651 Ghadames Basin, and corresponds to an episode of increased primary productivity and photic-
652 zone anoxia. Though ambiguity remains on the exact age of this radioactive shale interval, our
653 data suggest eutrophication was favored by the entrance of nutrient-rich waters into the
654 Ghadames Basin. The upper part of OA IV Fm. is marked by a facies change associated with
655 the Famennian regression. Photic zone anoxia was less frequent but the sediment is still
656 organic-rich because of increased delivery of terrestrial OM.

657 The Late Devonian was a period of important changes in the carbon cycle marked by
658 several episodes of oceanic anoxia and biotic crisis. While detailed and high-resolution
659 studies of Late Devonian events in European, Asian and North-American successions are
660 numerous, similar studies in North Gondwana remain rare and are mainly restricted to
661 Morocco and Algeria, where the sediments present relatively proximal depositional facies.
662 The present study demonstrates that the Ghadames Basin, in addition to its important
663 petroleum interest, contains a rich sedimentary succession prone to future high-resolution
664 studies of the Late Devonian events in North Gondwana.

665

666

667 **Acknowledgments**

668 This article is dedicated to the memory of Dominique Massa who provided the
669 samples and supported research in the Paleozoic of North Africa. Jonhatan Redfern
670 (University of Manchester) is acknowledged for providing detailed information on D1-26
671 borehole. This is a contribution to the project “The terrestrialization process: modeling
672 complex interaction at the biosphere–geosphere interface” financially supported by the INSU
673 ECLIPSE program, and the ANR TERRES project (ANR-10-BLAN-0607). Université de
674 Lille is acknowledged for a 12-month postdoctoral grant awarded to A. Spina. Nicolas Visez
675 and Sylvie Gosselin (PC2A, Université de Lille) are acknowledged for GC-MS injections.
676 Thomas Algeo, Grzegorz Racki and an anonymous reviewer are acknowledged for
677 constructive comments on the first version of this manuscript.

678

679

680

681 **Literature**

682 Alexander, R., Kagi, R., Noble, R. (1983) Identification of the bicyclic sesquiterpenes
683 drimane and eudesmane in petroleum. *Journal of the Chemical Society, Chemical*
684 *Communications*, 5, 226–228.

685 Algeo, T.J. (2004) Can marine anoxic events draw down the trace element inventory of
686 seawater? *Geology*, **32**, 12, 1057.

687 Algeo, T.J., Berner, R.A., Maynard, J.B., Scheckler, S.E. (1995) Late Devonian oceanic
688 anoxic events and biotic crises: “rooted” in the evolution of vascular land plants? *GSA Today*,
689 **5**, 3, 45, 64–66.

690 Algeo, T.J., Lyons, T.W. (2006) Mo–total organic carbon covariation in modern anoxic
691 marine environments: Implications for analysis of paleoredox and paleohydrographic
692 conditions. *Paleoceanography*, **21**, 1, PA1016.

693 Algeo, T.J., Scheckler, S.E. (1998) Terrestrial-marine teleconnections in the Devonian: links
694 between the evolution of land plants, weathering processes, and marine anoxic events.
695 *Philosophical Transactions of the Royal Society B: Biological Sciences*, **353**, 1365, 113–130.

696 Algeo, T.J., Tribovillard, N. (2009) Environmental analysis of paleoceanographic systems
697 based on molybdenum–uranium covariation. *Chemical Geology*, **268**, 3–4, 211–225.

698 Aquino Neto, F.R., Trigüis, J., Azevedo, D.A., Rodrigues, R., Simoneit, B.R.T. (1992)
699 Organic geochemistry of geographically unrelated tasmanites. *Organic Geochemistry*, **18**, 6,
700 791–803.

701 Armstrong, H.A., Abbott, G.D., Turner, B.R., Makhlof, I.M., Muhammad, A.B.,
702 Pedentchouk, N., Peters, H. (2009) Black shale deposition in an Upper Ordovician–Silurian
703 permanently stratified, peri-glacial basin, southern Jordan. *Organic-Carbon-Rich Sediments
704 through the Phanerozoic: Processes, Progress, and Perspectives*, **273**, 3, 368–377.

705 Averbuch, O., Tribovillard, N., Devleeschouwer, X., Riquier, L., Mistiaen, B., Van Vliet-
706 Lanoe, B. (2005) Mountain building-enhanced continental weathering and organic carbon
707 burial as major causes for climatic cooling at the Frasnian–Famennian boundary (c. 376 Ma)?
708 *Terra Nova*, **17**, 1, 25–34.

709 Becker, R.T., Gradstein, F.M., Hammer, O. (2012) Chapter 22 - The Devonian Period. *The
710 Geologic Time Scale*, Elsevier, Boston, pp. 559–601.

711 Becker, R.T., Königshof, P., Brett, C.E. (2016) *Devonian climate, sea level and evolutionary
712 events*. Geological Society of London, 481 p.

713 Behar, F., Beaumont, V., De B. Pentead, H.L. (2001) Technologie Rock-Eval 6 :
714 performances et développements. *Oil & Gas Science and Technology - Rev. IFP*, **56**, 2, 111–
715 134.

716 Behrens, A., Wilkes, H., Schaeffer, P., Clegg, H., Albrecht, P. (1998) Molecular
717 characterization of organic matter in sediments from the Keg River formation (Elk Point
718 group), western Canada sedimentary basin. *Organic Geochemistry*, **29**, 8, 1905–1920.

719 Berner, R.A. (1982) Burial of organic carbon and pyrite sulfur in the modern ocean: its
720 geochemical and environmental significance. *American Journal of Science*, **282**, 451–473.

721 Berner, R.A., Raiswell, R. (1983) Burial of organic carbon and pyrite sulfur in sediments over
722 Phanerozoic time: a new theory. *Geochimica et Cosmochimica Acta*, **47**, 855–862.

723 Bond, D., Wignall, P.B., Racki, G. (2004) Extent and duration of marine anoxia during the
724 Frasnian–Famennian (Late Devonian) mass extinction in Poland, Germany, Austria and
725 France. *Geological Magazine*, **141**, 2, 173–193.

726 Bond, D.P.G., Wignall, P.B. (2008) The role of sea-level change and marine anoxia in the
727 Frasnian–Famennian (Late Devonian) mass extinction. *Palaeogeography, Palaeoclimatology,*
728 *Palaeoecology*, **263**, 3, 107–118.

729 Boote, D.R.D., Clark-Lowes, D.D., Traut, M.W. (1998) Palaeozoic petroleum systems of
730 North Africa. *Geological Society, London, Special Publications*, **132**, 1, 7.

731 Bourbonniere, R.A., Meyers, P.A. (1996) Sedimentary geolipid records of historical changes
732 in the watersheds and productivities of Lakes Ontario and Erie. *Limnology and*
733 *Oceanography*, **41**, 2, 352–359.

734 Bray, E.E., Evans, E.D. (1961) Distribution of *n*-paraffins as a clue to recognition of source
735 beds. *Geochimica et Cosmochimica Acta*, **22**, 2–15.

736 Brown, E.T., Le Callonnec, L., German, C.R. (2000) Geochemical cycling of redox-sensitive
737 metals in sediments from Lake Malawi: a diagnostic paleotracer for episodic changes in
738 mixing depth. *Geochimica et Cosmochimica Acta*, **64**, 20, 3515–3523.

739 Buggisch, W. (1991) The global Frasnian-Famennian »Kellwasser Event«. *Geologische*
740 *Rundschau*, **80**, 1, 49–72.

741 Bushnev, D. (2009) Organic matter of the Ukhta domanik. *Doklady Earth Sciences*, **426**, 4,
742 1531–8354.

743 Canaple, J. (1963) *Synthèse régionale du sud-tunisien. Corrélations entre les forages BS1-*
744 *OSI-SNI-DNI-MG1-DI.26*. Compagnie Franco-tunisienne des pétroles,.

745 Carmichael, S.K., Waters, J.A., Suttner, T.J., Kido, E., DeReuil, A.A. (2014) A new model
746 for the Kellwasser Anoxia Events (Late Devonian): Shallow water anoxia in an open oceanic
747 setting in the Central Asian Orogenic Belt. *Palaeogeography, Palaeoclimatology,*
748 *Palaeoecology*, **399**, 394–403.

749 Carr, I.D. (2002) Second-order sequence stratigraphy of the Palaeozoic of North Africa.
750 *Journal of Petroleum Geology*, **25**, 3, 259–280.

751 Chen, D., Tucker, M.E. (2003) The Frasnian–Famennian mass extinction: insights from high-
752 resolution sequence stratigraphy and cyclostratigraphy in South China. *Palaeogeography,*
753 *Palaeoclimatology, Palaeoecology*, **193**, 1, 87–111.

754 Clifford, D.J., Clayton, J.L., Sinnighe Damsté, J.S. (1998) 2,3,6-/3,4,5-Trimethyl substituted
755 diaryl carotenoid derivatives (Chlorobiaceae) in petroleums of the Belarussian Pripyat River
756 Basin. *Organic Geochemistry*, **29**, 5–7, 1253–1267.

757 Colbath, G.K., Grenfell, H.R. (1995) Review of biological affinities of Paleozoic acid-
758 resistant, organic-walled eukaryotic algal microfossils (including “acritarchs”). *Review of*
759 *Palaeobotany and Palynology*, **86**, 3, 287–314.

760 Craig, J., Rizzi, C., Said, F., Thusu, B., Lüning, S., Asbali, A.I., Keeley, M.L., Bell, J.F.,
761 Durham, M.J., Eales, M.H., et al. (2008) Structural styles and prospectivity in the
762 Precambrian and Palaeozoic hydrocarbon systems of North Africa. In : Salem, M.J., Oun,
763 K.M., Essed, A.S., (eds.). *The Geology of East Libya, Vol. IV*, pp. 51–122.

764 Cullers, R.L., Podkovyrov, V.N. (2002) The source and origin of terrigenous sedimentary
765 rocks in the Mesoproterozoic Ui group, southeastern Russia. *Precambrian Research*, **117**, 3–
766 4, 157–183.

767 Dardour, A.M., Boote, D.R.D., Baird, A.W. (2004) Stratigraphic controls on Palaeozoic
768 petroleum systems, Ghadames Basin, Libya. *Journal of Petroleum Geology*, **27**, 2, 141–162.

769 Dutta, S., Greenwood, P.F., Brocke, R., Schaefer, R.G., Mann, U. (2006) New insights into
770 the relationship between *Tasmanites* and tricyclic terpenoids. *Organic Geochemistry*, **37**, 1,
771 117–127.

772 Echikh, K. (1998) Geology and hydrocarbon occurrences in the Ghadames Basin, Algeria,
773 Tunisia, Libya. *Geological Society, London, Special Publications*, **132**, 1, 109.

774 Eglinton, G., Hamilton, R.J. (1967) Leaf epicuticular waxes. *Science*, **156**, 3780, 1322–1335.

775 Evitt, W.R. (1963) A discussion and proposals concerning fossil dinoflagellates,
776 hystrichospheres, and acritarchs, I. *Proceedings of the National Academy of Sciences*, **49**, 2,
777 158–164.

778 Farrimond, P., Telnæs, N. (1996) Three series of rearranged hopanes in Toarcian sediments
779 (northern Italy). *Organic Geochemistry*, **25**, 3–4, 165–177.

780 Filipiak, P. (2002) Palynofacies around the Frasnian/Famennian boundary in the Holy Cross
781 Mountains, southern Poland. *Palaeogeography, Palaeoclimatology, Palaeoecology*, **181**, 1–3,
782 313–324.

783 French, K.L., Rocher, D., Zumberge, J.E., Summons, R.E. (2015) Assessing the distribution
784 of sedimentary C₄₀ carotenoids through time. *Geobiology*, **13**, 2, 139–151.

785 Frizon de Lamotte, D., Tavakoli-Shirazi, S., Leturmy, P., Averbuch, O., Mouchot, N., Raulin,
786 C., Leparmentier, F., Blanpied, C., Ringenbach, J.-C. (2013) Evidence for Late Devonian
787 vertical movements and extensional deformation in northern Africa and Arabia: Integration in
788 the geodynamics of the Devonian world. *Tectonics*, **32**, 2, 107–122.

789 Gelpi, E., Schneider, H., Mann, J., Oro, J. (1970) Hydrocarbons of geochemical significance
790 in microscopic algae. *Phytochemistry*, **9**, 3, 603–612.

791 Godderis, Y., Joachimski, M.M. (2004) Global change in the Late Devonian: modelling the
792 Frasnian-Famennian short-term carbon isotope excursions. *Palaeogeography,*
793 *Palaeoclimatology, Palaeoecology*, **202**, 3–4, 309–329.

794 Greenwood, P.F., George, S.C. (1999) Mass spectral characteristics of C₁₉ and C₂₀ tricyclic
795 terpanes detected in Latrobe Tasmanite oil shale. *European Mass Spectrometry*, **5**, 3, 221–
796 230.

797 Guiraud, R., Bosworth, W., Thierry, J., Delplanque, A. (2005) Phanerozoic geological
798 evolution of Northern and Central Africa: An overview. *Phanerozoic Evolution of Africa*, **43**,
799 *I*, 83–143.

800 Haddad, E.E., Tuite, M.L., Martinez, A.M., Williford, K., Boyer, D.L., Droser, M.L., Love,
801 G.D. (2016) Lipid biomarker stratigraphic records through the Late Devonian
802 Frasnian/Famennian boundary: Comparison of high- and low-latitude epicontinental marine
803 settings. *Organic Geochemistry*, **98**, 38–53.

804 Haq, B.U., Schutter, S.R. (2008) A chronology of Paleozoic sea-level changes. *Science*, **322**,
805 *5898*, 64.

806 Hart, G.F. (1986) Origin and classification of organic matter in clastic systems. *Palynology*,
807 **10**, *I*, 1.

808 Hartgers, W.A., Sinninghe Damsté, J.S., Requejo, A.G., Allan, J., Hayes, J.M., Ling, Y., Xie,
809 T.-M., Primack, J., de Leeuw, J.W. (1994) A molecular and carbon isotopic study towards the
810 origin and diagenetic fate of diaromatic carotenoids. *Organic Geochemistry*, **22**, 3, 703–725.

811 Hauke, V., Wehrung, P., Hussler, G., Trendel, J.M., Albrecht, P., Riva, A., Connan, J. (1993)
812 Rearranged des-*E*-hopanoid hydrocarbons in sediments and petroleum. *Organic*
813 *Geochemistry*, **20**, 3, 415–423.

814 House, M.R. (2002) Strength, timing, setting and cause of mid-Palaeozoic extinctions.
815 *Palaeogeography, Palaeoclimatology, Palaeoecology*, **181**, 1–3, 5–25.

816 Hrouda, M. (2004) The hydrocarbon source potential of the Palaeozoic rocks of the
817 Ghadames Basin, NW Libya. Newcastle University.

818 Joachimski, M.M., Buggisch, W. (1993) Anoxic events in the late Frasnian—Causes of the
819 Frasnian-Famennian faunal crisis? *Geology*, **21**, 8, 675–678.

820 Joachimski, M.M., Buggisch, W. (2002) Conodont apatite $\delta^{18}\text{O}$ signatures indicate climatic
821 cooling as a trigger of the Late Devonian mass extinction. *Geology*, **30**, 8, 711.

822 Joachimski, M.M., Ostertag-Henning, C., Pancost, R.D., Strauss, H., Freeman, K.H., Littke,
823 R., Sinninghe Damsté, J.S., Racki, G. (2001) Water column anoxia, enhanced productivity

824 and concomitant changes in $\delta^{13}\text{C}$ and $\delta^{34}\text{S}$ across the Frasnian-Famennian boundary (Kowala
825 - Holy Cross Mountains/Poland). *Chemical Geology*, **175**, 1–2, 109–131.

826 Johnson, J.G., Klapper, G., Sandberg, C.A. (1985) Devonian eustatic fluctuations in
827 Euramerica. *GSA Bulletin*, **96**, 5, 567–587.

828 Kashirtsev, V.A., Moskvina, V.I., Fomin, A.N., Chalaya, O.N. (2010) Terpanes and steranes in
829 coals of different genetic types in Siberia. *Russian Geology and Geophysics*, **51**, 4, 404–411.

830 Koopmans, M.P., Köster, J., Van Kaam-Peters, H.M.E., Kenig, F., Schouten, S., Hartgers,
831 W.A., de Leeuw, J.W., Sinninghe Damsté, J.S. (1996) Diagenetic and catagenetic products of
832 isorenieratene: Molecular indicators for photic zone anoxia. *Geochimica et Cosmochimica*
833 *Acta*, **60**, 22, 4467–4496.

834 Leventhal, J.S. (1983) An interpretation of carbon and sulfur relationships in Black Sea
835 sediments as indicators of environments of deposition. *Geochimica et Cosmochimica Acta*,
836 **47**, 133–137.

837 Liaaen-Jensen, S. (1978) Marine carotenoids. In : Scheuer, P.J., (ed.). *Marine Natural*
838 *Products, Chemical and Biological Perspectives*, Academic Press, pp. 1–73.

839 Loboziak, S., Streel, M. (1989) Middle-upper Devonian miospores from the Ghadamis Basin
840 (Tunisia-Libya): Systematics and stratigraphy. *Review of Palaeobotany and Palynology*, **58**,
841 2–4, 173–196.

842 Lu, H., Chen, T., Grice, K., Greenwood, P., Peng, P., Sheng, G. (2009) Distribution and
843 significance of novel low molecular weight steranes in an immature evaporitic sediment from
844 the Jinxian Sag, North China. *Organic Geochemistry*, **40**, 8, 902–911.

845 Lüning, S., Adamson, K., Craig, J. (2003) Frasnian organic-rich shales in North Africa:
846 regional distribution and depositional model. *Geological Society, London, Special*
847 *Publications*, **207**, 1, 165.

848 Lüning, S., Wendt, J., Belka, Z., Kaufmann, B. (2004) Temporal–spatial reconstruction of the
849 early Frasnian (Late Devonian) anoxia in NW Africa: new field data from the Ahnet Basin
850 (Algeria). *Sedimentary Geology*, **163**, 3, 237–264.

851 Martin, F. (1993) Acritarchs: a review. *Biological Reviews*, **68**, 4, 475–537.

852 Martín-Closas, C. (2003) The fossil record and evolution of freshwater plants: A review.
853 *Geologica Acta*, **1**, 4, 315–338.

854 Marynowski, L., Simoneit, B.R.T. (2009) Widespread Upper Triassic to Lower Jurassic
855 wildfire records from Poland: evidence from charcoal and pyrolytic polycyclic aromatic
856 hydrocarbons. *Palaios*, **24**, 12, 785–798.

857 Marynowski, L., Zatoń, M., Rakociński, M., Filipiak, P., Kurkiewicz, S., Pearce, T.J. (2012)
858 Deciphering the upper Famennian Hangenberg Black Shale depositional environments based
859 on multi-proxy record. *Palaeogeography, Palaeoclimatology, Palaeoecology*, **346**, 66–86.

860 Maslen, E., Grice, K., Gale, J.D., Hallmann, C., Horsfield, B. (2009) Crocetane: A potential
861 marker of photic zone euxinia in thermally mature sediments and crude oils of Devonian age.
862 *Organic Geochemistry*, **40**, 1, 1–11.

863 Massa, D. (1988) Paléozoïque de Libye occidentale : stratigraphie et paléogéographie.

864 McGhee, G.R., Clapham, M.E., Sheehan, P.M., Bottjer, D.J., Droser, M.L. (2013) A new
865 ecological-severity ranking of major Phanerozoic biodiversity crises. *Palaeogeography,*
866 *Palaeoclimatology, Palaeoecology*, **370**, 260–270.

867 McLennan, S.M. (1989) Rare earth elements in sedimentary rocks; influence of provenance
868 and sedimentary processes. *Reviews in Mineralogy and Geochemistry*, **21**, 1, 169–200.

869 Melendez, I., Grice, K., Trinajstić, K., Ladjavardi, M., Greenwood, P., Thompson, K. (2013)
870 Biomarkers reveal the role of photic zone euxinia in exceptional fossil preservation: An
871 organic geochemical perspective. *Geology*, **41**, 2, 123–126.

872 Meyers, P. (1997) Organic geochemical proxies of paleoceanographic, paleolimnologic, and
873 paleoclimatic processes. *Organic Geochemistry*, **27**, 5/6, 213–250.

874 Moldowan, J.M., Dahl, J., Jacobson, S.R., Huizinga, B.J., Fago, F.J., Shetty, R., Watt, D.S.,
875 Peters, K.E. (1996) Chemostratigraphic reconstruction of biofacies: molecular evidence
876 linking cyst-forming dinoflagellates with pre-Triassic ancestors. *Geology*, **24**, 2, 159–162.

877 Moldowan, J.M., Fago, F.J., Carlson, R.M.K., Young, D.C., an Duvne, G., Clardy, J., Schoell,
878 M., Pillinger, C.T., Watt, D.S. (1991) Rearranged hopanes in sediments and petroleum.
879 *Geochimica et Cosmochimica Acta*, **55**, 11, 3333–3353.

880 Moldowan, J.M., Talyzina, N.M. (1998) Biogeochemical evidence for dinoflagellate
881 ancestors in the Early Cambrian. *Science*, **281**, 1168–1170.

882 Mongelli, G. (1995) Trace elements distribution and mineralogical composition in the < 2- μ m
883 size fraction of shales from the Southern Apennines, Italy. *Mineralogy and Petrology*, **53**, 1–
884 3, 103–114.

885 Murphy, A.E., Sageman, B.B., Hollander, D.J., Lyons, T.W., Brett, C.E. (2000) Black shale
886 deposition and faunal overturn in the Devonian Appalachian Basin: Clastic starvation,
887 seasonal water-column mixing, and efficient biolimiting nutrient recycling.
888 *Paleoceanography*, **15**, 3, 280–291.

889 Oasis oils Company (1961) D1-26 final log.

890 Ourisson, G., Albrech, P., Rohmer, M. (1979) The hopanoids - Paleochemistry and
891 biochemistry of a group of natural products. *Pure and Applied Chemistry*, **51**, 4, 709–729.

892 Overmann, J. (2008) Ecology of phototrophic sulfur bacteria. In : Hell, R., Dahl, C., Knaff,
893 D., Leustek, T., (eds.). *Sulfur Metabolism in Phototrophic Organisms*, Springer Netherlands,
894 Dordrecht, pp. 375–396.

895 Overmann, J., Cypionka, H., Pfennig, N. (1992) An extremely low-light adapted phototrophic
896 sulfur bacterium from the Black Sea. *Limnology and Oceanography*, **37**, 1, 150–155.

897 Paris, F., Nölvak, J. (1999) Biological interpretation and paleobiodiversity of a cryptic fossil
898 group: The “chitinozoan animal.” *Geobios*, **32**, 2, 315–324.

899 Peters, K.E., Walters, C.W., Moldowan, J.M. (2005) *The biomarker guide, second edition*.
900 Cambridge University Press, Cambridge, 1155 p.

901 Peterson, L.C., Haug, G.H., Murray, R.W., Yarincik, K.M., King, J.W., Bralower, T.J.,
902 Kameo, K., Rutherford, S.D., Pearce, R.B. (2000) Late Quaternary stratigraphy and
903 sedimentation at ODP Site 1002, Cariaco Basin (Venezuela). In : Leckie, R.M., Sigurdsson,
904 H., Acton, G.D., Draper, G., (eds.). *Proceedings of the ODP, Scientific Results*, pp. 85–99.

905 Prauss, M.L. (2007) Availability of reduced nitrogen chemospecies in photic-zone waters as
906 the ultimate cause for fossil prasinophyte prosperity. *Palaios*, **22**, 5, 489–499.

907 Racka, M., Marynowski, L., Filipiak, P., Sobstel, M., Piszczowska, A., Bond, D.P.G. (2010)
908 Anoxic Annulata Events in the Late Famennian of the Holy Cross Mountains (Southern
909 Poland): Geochemical and palaeontological record. *Palaeogeography, Palaeoclimatology,*
910 *Palaeoecology*, **297**, 3, 549–575.

911 Racki, G. (2005) Toward understanding Late Devonian global events: few answers, many
912 questions. In : Over, D.J., Morrow, J.R., Wignall, P.B., (eds.). *Understanding Late Devonian*
913 *and Permian-Triassic Biotic and Climatic Events: Towards an Integrated Approach*, Elsevier,
914 pp. 5–36.

915 Radke, M., Welte, D.H. (1983) The Methylphenanthrene Index (MPI): a maturity parameter
916 based on aromatic hydrocarbons. In : Bjorøy, P., Albrecht, P., Cornford, C., (eds.). *Advances*
917 *in Organic Geochemistry 1981*, Wiley, Chichester, pp. 504–512.

918 Radke, M., Willsch, H., Leythaeuser, D., Teichmüller, M. (1982) Aromatic components of
919 coal: relation of distribution pattern to rank. *Geochimica et Cosmochimica Acta*, **46**, 10,
920 1831–1848.

921 Requejo, A.G., Allan, J., Creaney, S., Gray, N.R., Cole, K.S. (1992) Aryl isoprenoids and
922 diaromatic carotenoids in Paleozoic source rocks and oils from the Western Canada and
923 Williston Basins. *Organic Geochemistry*, **19**, 1–3, 245–264.

924 Riboulleau, A., Bout-Roumazielles, V., Tribovillard, N., Guillot, F., Recourt, P. (2014)
925 Testing provenance diagrams: Lessons from the well-constrained Cariaco Basin. *Chemical*
926 *Geology*, **389**, 91–103.

927 Riquier, L., Averbuch, O., Devleeschouwer, X., Tribovillard, N. (2010) Diagenetic versus
928 detrital origin of the magnetic susceptibility variations in some carbonate Frasnian–
929 Famennian boundary sections from Northern Africa and Western Europe: implications for
930 paleoenvironmental reconstructions. *International Journal of Earth Sciences*, **99**, 1, 57–73.

931 Riquier, L., Tribovillard, N., Averbuch, O., Devleeschouwer, X., Riboulleau, A. (2006) The
932 Late Frasnian Kellwasser horizons of the Harz Mountains (Germany): Two oxygen-deficient
933 periods resulting from different mechanisms. *Chemical Geology*, **233**, 1–2, 137–155.

934 Riquier, L., Tribovillard, N., Averbuch, O., Joachimski, M.M., Racki, G., Devleeschouwer,
935 X., El albani, A., Riboulleau, A. (2005) Productivity and bottom water redox conditions at the
936 Frasnian-Famennian boundary on both sides of the Eovariscan Belt: constraints from trace-
937 element geochemistry. *Understanding Late Devonian And Permian-Triassic Biotic and*
938 *Climatic Events Towards an Integrated Approach*, Elsevier, pp. 199–224.

939 Romero-Sarmiento, M.-F., Riboulleau, A., Vecoli, M., Versteegh, G.J.-M. (2011) Aliphatic
940 and aromatic biomarkers from Gondwanan sediments of Late Ordovician to Early Devonian
941 age: An early terrestrialization approach. *Organic Geochemistry*, **42**, 6, 605–617.

942 de la Rue, S.R., Rowe, H.D., Rimmer, S.M. (2007) Palynological and bulk geochemical
943 constraints on the paleoceanographic conditions across the Frasnian–Famennian boundary,
944 New Albany Shale, Indiana. *International Journal of Coal Geology*, **71**, 1, 72–84.

945 Sandberg, C.A., Morrow, J.R., Ziegler, W. (2002) Late Devonian sea-level changes,
946 catastrophic events, and mass extinctions. In : Koeberl, C., MacLeod, K.G., (eds.).
947 *Catastrophic Events and Mass Extinctions: Impacts and Beyond*, Geological Society of
948 America, p.

949 Schieber, J., Lazar, R.O. (2004) *Devonian black shales of the eastern U.S.: New insights into*
950 *sedimentology and stratigraphy from the subsurface and outcrops in the Illinois and*
951 *Appalachian Basins*. Indiana Geological Survey, Bloomington, Ind., 90 p.

952 Schwark, L., Emt, P. (2006) Sterane biomarkers as indicators of palaeozoic algal evolution
953 and extinction events. *Evolution of the System Earth in the Late Palaeozoic: Clues from*
954 *Sedimentary Geochemistry*, **240**, 1, 225–236.

955 Schwark, L., Frimmel, A. (2004) Chemostratigraphy of the Posidonia Black Shale, SW-
956 Germany: II. Assessment of extent and persistence of photic-zone anoxia using aryl
957 isoprenoid distributions. *Chemical Geology*, **206**, 3–4, 231–248.

958 Sephton, M.A., Looy, C.V., Veeffkind, R.J., Visscher, H., Brinkhuis, H., de Leeuw, J.W.
959 (1999) Cyclic diaryl ethers in a Late Permian sediment. *Organic Geochemistry*, **30**, 4, 267–
960 273.

961 Soua, M. (2014) Paleozoic oil/gas shale reservoirs in southern Tunisia: An overview. *Journal*
962 *of African Earth Sciences*, **100**, 450–492.

963 Spina, A., Vecoli, M., Riboulleau, A., Clayton, G., Cirilli, S., Di Michele, A., Marcoguisseppe,
964 A., Rettori, R., Sassi, P., Servais, T., et al. (2017) *Assessment of thermal maturity of organic*
965 *matter of Lower Palaeozoic rocks (Ghadamis Basin, North Africa): application of*
966 *Palynomorph Darkness Index (PDI) and other thermal maturity indicators*. Perugia-Italy,.

967 Steemans, P. (1999) Paléodiversification des spores et des cryptospores de l'Ordovicien au
968 Dévonien inférieur. *Geobios*, **32**, 2, 341–352.

969 Streel, M. (2009) Upper Devonian miospore and conodont zone correlation in western
970 Europe. *Geological Society, London, Special Publications*, **314**, 1, 163.

971 Strother, P.K. (1991) A classification schema for the cryptospores. *Palynology*, **15**, 1, 219–
972 236.

973 Summons, R.E., Powell, T.G. (1986) Chlorobiaceae in Palaeozoic seas revealed by biological
974 markers, isotopes and geology. *Nature*, **319**, 6056, 763–765.

975 Tappan, H.N. (1980) *The paleobiology of plant protists*. W. H. Freeman,.

976 Taylor, T.N., Taylor, E.L., Krings, M. (2009) *Paleobotany: The Biology and Evolution of*
977 *Fossil Plants*. Academic Press, 1230 p.

978 Tribovillard, N. (2013) The Ge/Si ratio as a tool to recognize biogenic silica in chert. *Comptes*
979 *Rendus Geoscience*, **345**, 3, 160–165.

980 Tribovillard, N., Averbuch, O., Devleeschouwer, X., Racki, G., Riboulleau, A. (2004) Deep-
981 water anoxia over the Frasnian–Famennian boundary (La Serre, France): a tectonically
982 induced oceanic anoxic event? *Terra Nova*, **16**, 5, 288–295.

983 Tribovillard, N., Bout-Roumazielles, V., Algeo, T., Lyons, T.W., Sionneau, T., Montero-
984 Serrano, J.C., Riboulleau, A., Baudin, F. (2008) Paleodepositional conditions in the Orca
985 Basin as inferred from organic matter and trace metal contents. *Marine Geology*, **254**, 1–2,
986 62–72.

987 Tulipani, S., Grice, K., Greenwood, P.F., Haines, P.W., Sauer, P.E., Schimmelmann, A.,
988 Summons, R.E., Foster, C.B., Böttcher, M.E., Playton, T., et al. (2015) Changes of
989 palaeoenvironmental conditions recorded in Late Devonian reef systems from the Canning
990 Basin, Western Australia: A biomarker and stable isotope approach. *Gondwana Research*, **28**,
991 4, 1500–1515.

992 Tyson, R.V. (1995) *Sedimentary organic matter*. Chapman & Hall, London., 615 p.
993 Ulmishek, G.F., Klemme, H.D. (1990) *Depositional controls, distribution, and effectiveness*
994 *of world petroleum source rocks*.
995 Underdown, R., Redfern, J., Lisker, F. (2007) Constraining the burial history of the
996 Ghadames Basin, North Africa: an integrated analysis using sonic velocities, vitrinite
997 reflectance data and apatite fission track ages. *Basin Research*, **19**, 4, 557–578.
998 Vandembroucke, T.R.A., Armstrong, H.A., Williams, M., Paris, F., Sabbe, K., Zalasiewicz,
999 J.A., Nölvak, J., Verniers, J. (2010) Epipelagic chitinozoan biotopes map a steep latitudinal
1000 temperature gradient for earliest Late Ordovician seas: Implications for a cooling Late
1001 Ordovician climate. *Early Palaeozoic Palaeoenvironments*, **294**, 3, 202–219.
1002 Versteegh, G.J.M., Riboulleau, A. (2010) An organic geochemical perspective on
1003 terrestrialization. *Geological Society, London, Special Publications*, **339**, 1, 11–36.
1004 Wang, T.-G., Simoneit, B.R.T. (1995) Tricyclic terpanes in Precambrian bituminous
1005 sandstone from the eastern Yanshan region, North China. *Chemical Geology*, **120**, 1, 155–
1006 170.
1007 Wendt, J., Belka, Z. (1991) Age and depositional environment of upper devonian (early
1008 Frasnian to early famennian) black shales and limestones (Kellwasser facies) in the eastern
1009 Anti-Atlas, Morocco. *Facies*, **25**, 1, 51–89.
1010 Wendt, J., Kaufmann, B., Belka, Z., Klug, C., Lubeseder, S. (2006) Sedimentary evolution of
1011 a Palaeozoic basin and ridge system: the Middle and Upper Devonian of the Ahnet and
1012 Mouydir (Algerian Sahara). *Geological Magazine*, **143**, 3, 269.
1013 Weyant, M., Massa, D. (1991) Contribution of conodonts to the Devonian biostratigraphy of
1014 Western Libya. In : Salem, M.J., Hammuda, O.S., Eliagoubi, B.A., (eds.). *The Geology of*
1015 *Libya*, Elsevier, Amsterdam, pp. 1297–1322.
1016 Whitaker, M.F. (1984) The usage of palynology in definition of Troll Field geology. In:
1017 Reduction of uncertainties in innovative reservoir geomodelling. *6th Offshore Northern Seas*
1018 *Conference and Exhibition*, Norsk petroleum forening, Stavanger, pp. 1–50.
1019 Wilde, P., Quinby-Hunt, M.S., Erdtmann, B.-D. (1996) The whole-rock cerium anomaly: a
1020 potential indicator of eustatic sea-level changes in shales of the anoxic facies. *Sedimentary*
1021 *Geology*, **101**, 1–2, 43–53.

1022

1023

1024

1025 **Figure captions**

1026

1027 Figure 1: Location map of the Ghadames Basin showing the location of borehole D1-26.

1028

1029 Figure 2: Lithological and stratigraphic description of the Upper Devonian formations in
1030 borehole D1-26, with sonic and resistivity (ILD) curves (unavailable scale). Compilation of
1031 data from Oasis oils Company (1961), Canaple (1963) Loboziak and Streel (1989), Weyant
1032 and Massa (1991) Spina et al. (2017). The peaks in the ILD curve (grey area) underline an
1033 alternance of shale and limestones corresponding to the radioactive shales and Cues
1034 Limestone horizon.

1035

1036 Figure 3: Palynofacies observations of the samples from borehole D1-26. A) Particle
1037 counting; B,C) Prasinophycean cysts, AOM and acritarchs (B: slide 7802; C: slide 7780); D)
1038 Prasinophycean cysts and AOM (slide 7704); E) miospores, Prasinophycean cysts and
1039 palynomacerals (slide 7083). Photographs show the >50 μ m palynological residue. Legend of
1040 the log as in fig. 2.

1041

1042 Figure 4: Rock-Eval and bulk geochemistry of samples from borehole D1-26. A) Hydrogen
1043 index (HI) *versus* Tmax plot showing the type and maturity of the organic matter. B) Total
1044 sulfur *versus* total organic carbon (TOC) of the sediment. The dotted line corresponds to the
1045 relationship observed in “normal marine” shales (Berner, 1982; Berner and Raiswell, 1983).
1046 C) Same as B after doubling the TOC content in order to account for thermal loss of organic
1047 matter.

1048

1049 Figure 5: Mineral redox proxies in the samples from borehole D1-26. A) Enrichment factor
1050 (EF) of the main redox-sensitive trace elements. B) Cerium anomaly. The grey interval
1051 corresponds to the Cues Limestone horizon and radioactive shales.

1052

1053 Figure 6: Detrital proxies in the samples from borehole D1-26. A) major and trace element
1054 content normalized to the aluminum content. B) Rare earth element ratios and europium
1055 anomaly. The grey interval corresponds to the Cues Limestone horizon and radioactive shales.

1056

1057 Figure 7: Rare earth element content in the samples from borehole D1-26 normalized to the
1058 Post Archean Average Shale (PAAS, McLennan, 1989).

1059

1060 Figure 8: Representative fragmentograms showing the biomarker distribution in the aliphatic
1061 fraction of the extracts from borehole D1-26 samples. A) *n*-alkanes and linear isoprenoids
1062 (m/z 57; sample 7087). B) Di- and tri-cyclic terpenoids (m/z 123; sample 7087). C)
1063 Cheilantanes and hopanoids (m/z 191; sample 7085). D) Steroids and diasteroids (m/z 217;
1064 sample 7780). Numbers above symbols indicate carbon number.

1065

1066 Figure 9: Example of distribution of isorenieratene and palaerenieratene derivatives in the
1067 aromatic fraction of the extracts from borehole D1-26 samples (m/z 133+134; sample 7810).

1068

1069 Figure 10: Molecular indicators of redox conditions in the extracts from D1-26 samples. A)
1070 Total concentration of isorenieratene and palaerenieratene derivatives in the extracts. B) C₁₆-
1071 C₃₁ palaerenieratene to isorenieratene derivatives ratio (PIR). The grey interval corresponds to
1072 the Cues Limestone horizon and radioactive shales. C) Pristane to phytane ratio (Pr/Ph) versus
1073 the modified aryl isoprenoid ratio (AIR*). Scheme from Schwark and Frimmel (2004)

1074

1075 Figure 11: Depositional model for organic matter in the Ghadames Basin during the Frasnian
1076 to upper Famennian interval. See text for explanations.

1077

1078 **Supplementary material**

1079 Table S1: major, trace and rare earth element content in samples from borehole D1-26.

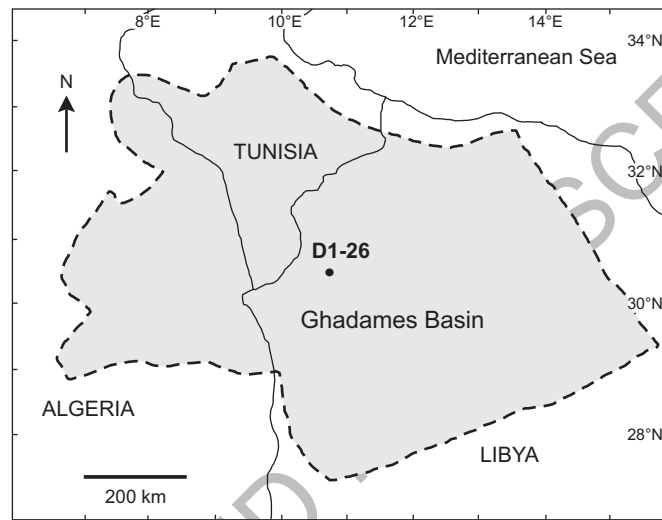


Figure 1

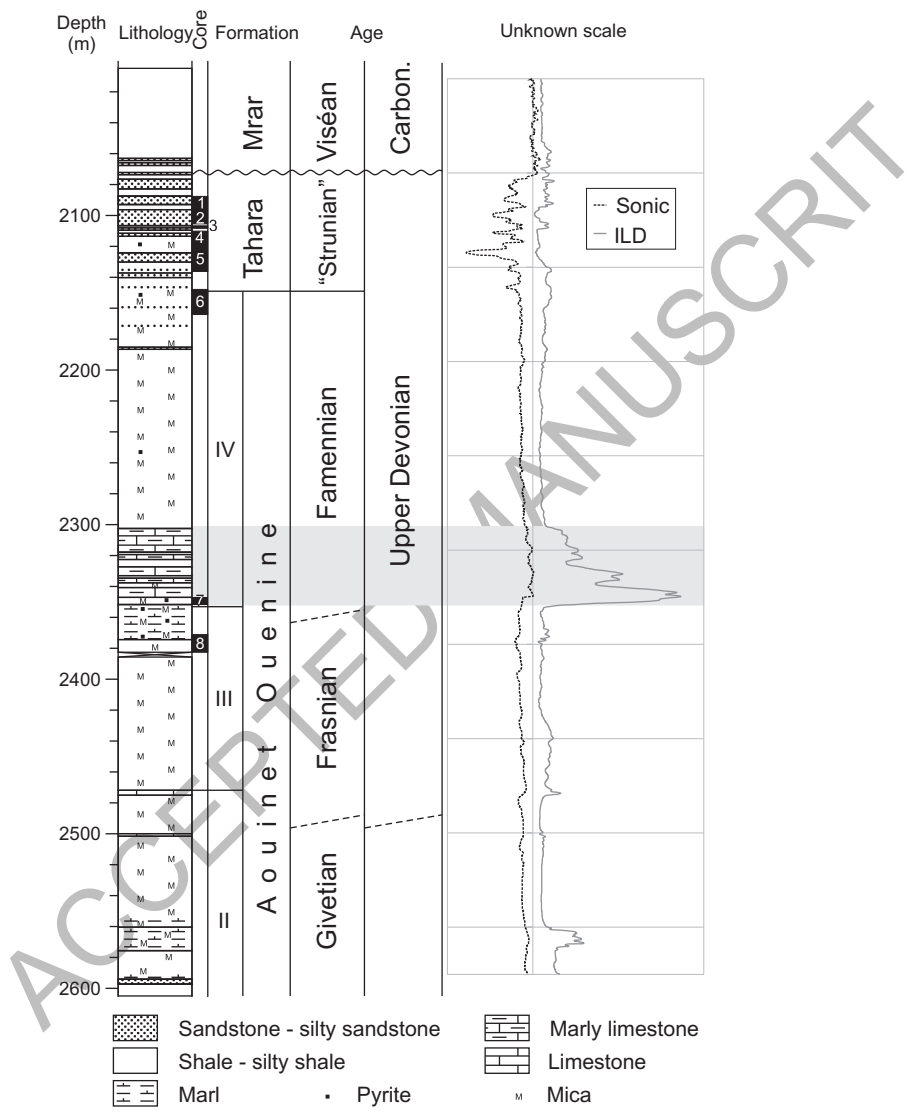


Figure 2

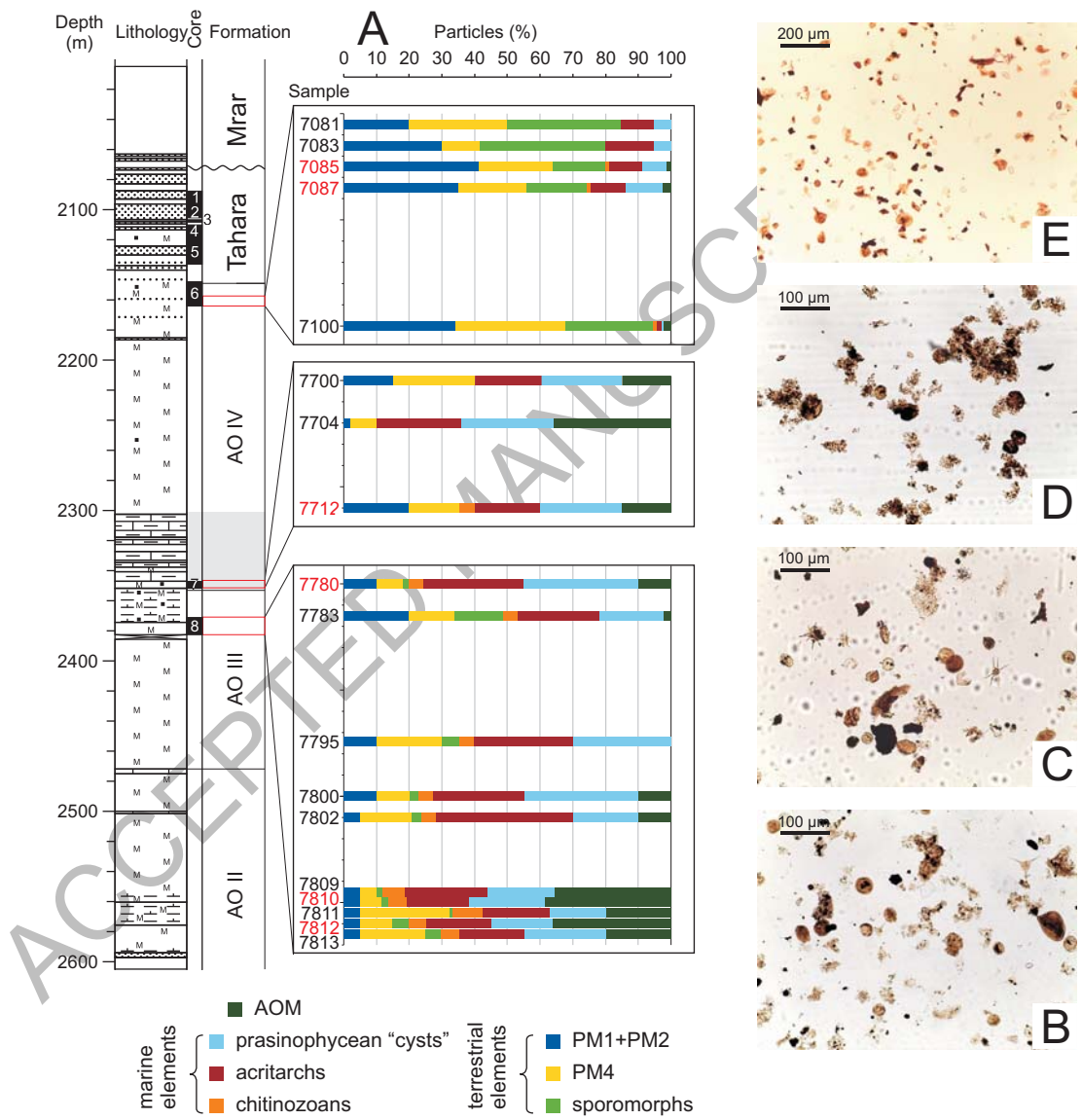


Figure 3

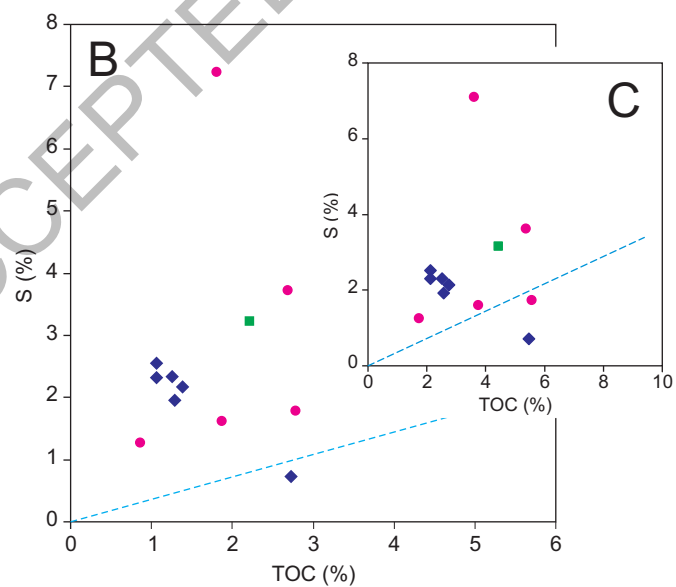
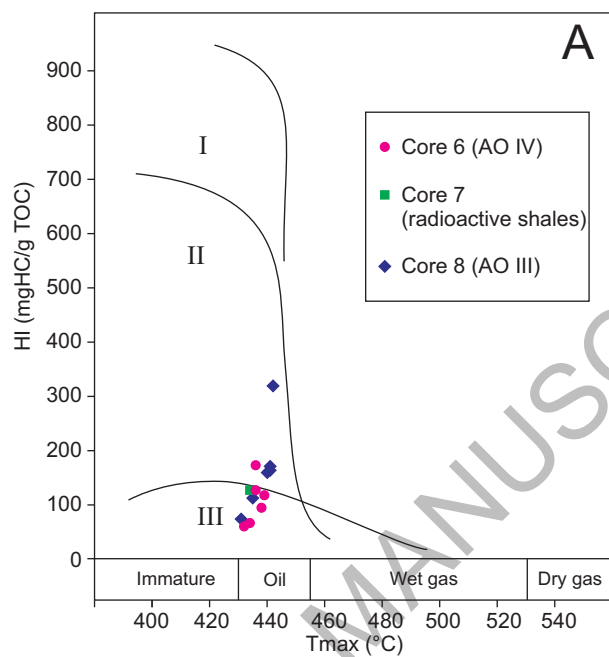


Figure 4

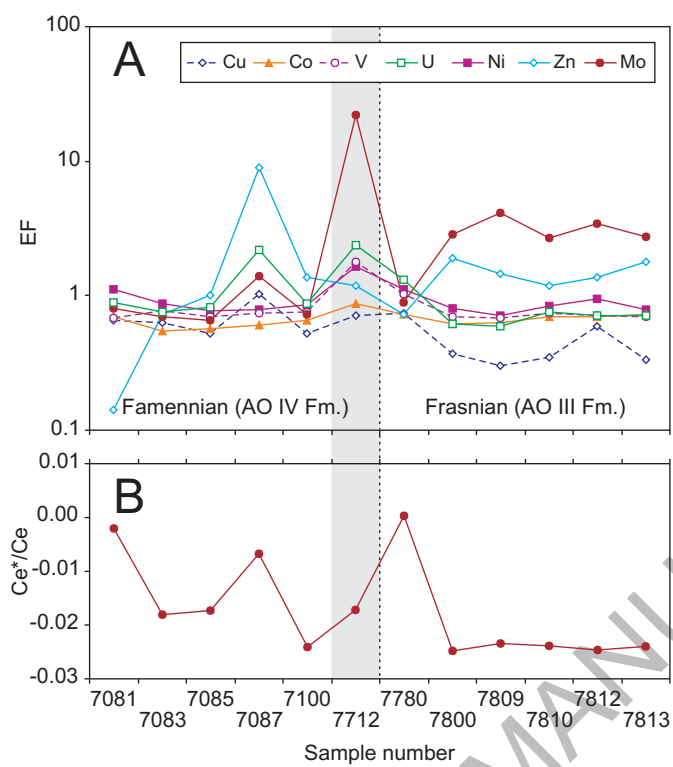


Figure 5

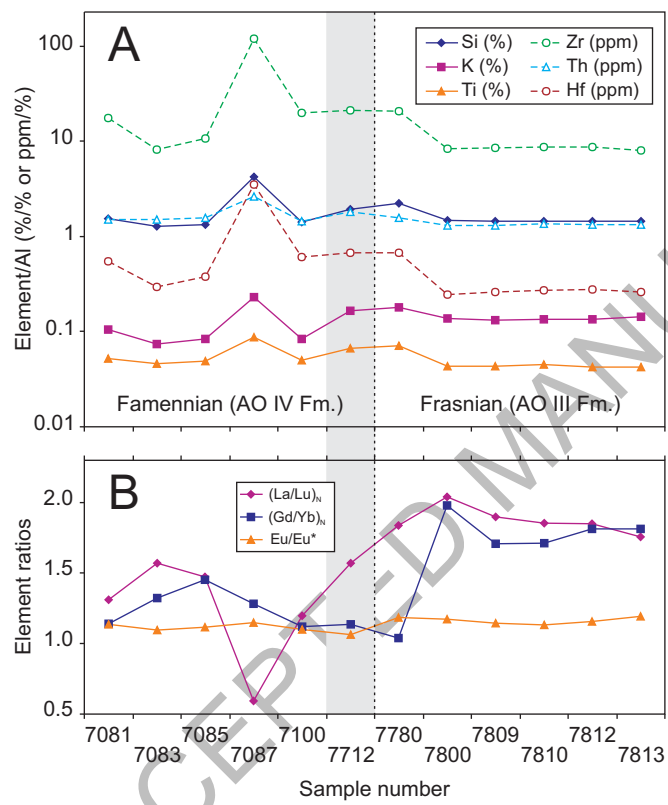


Figure 6

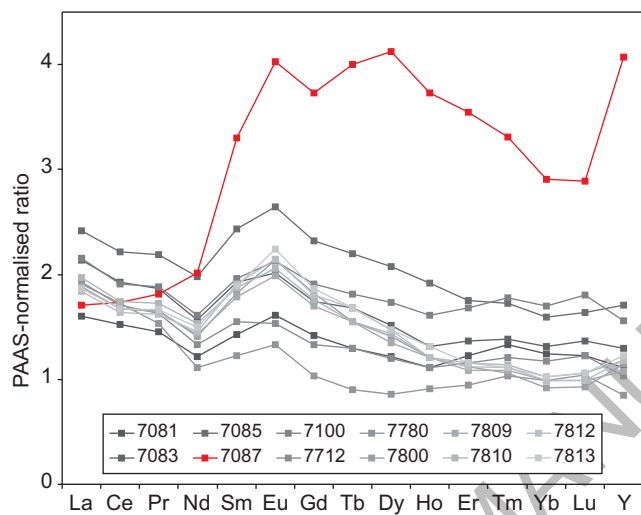


Figure 7

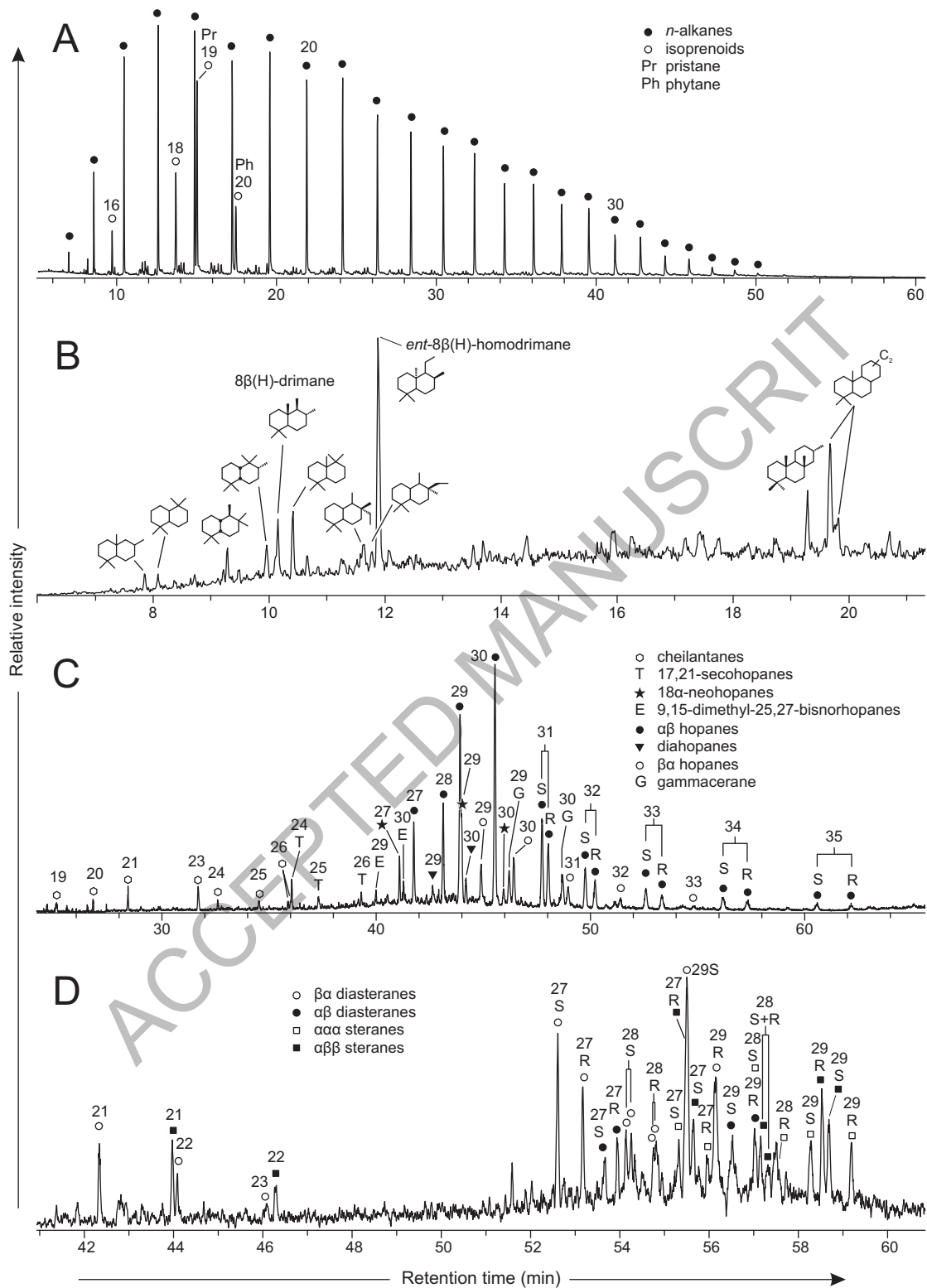


Figure 8

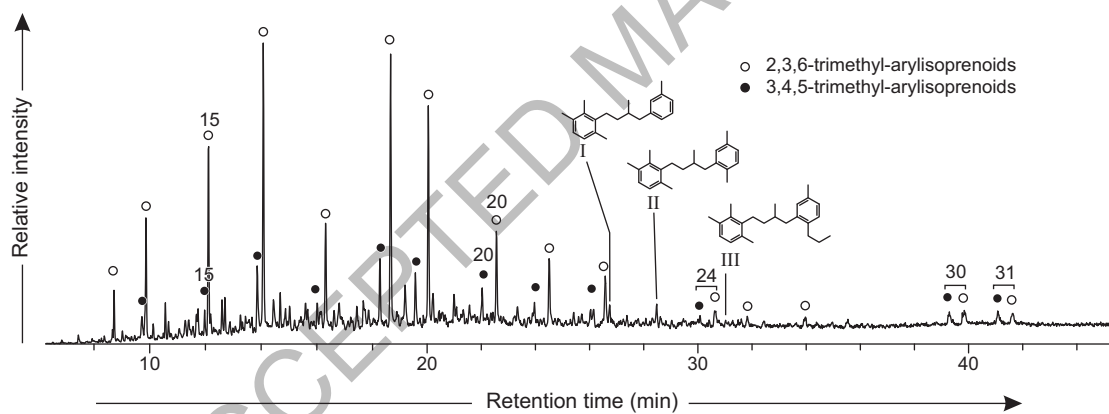


Figure 9

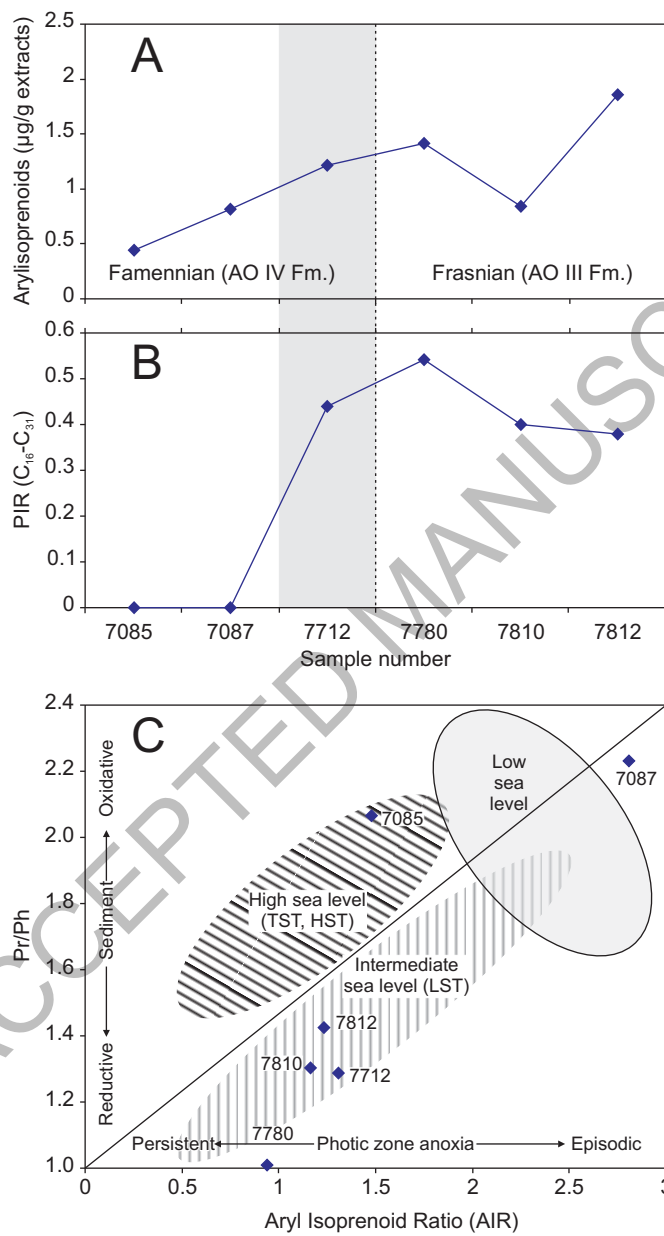


Figure 10

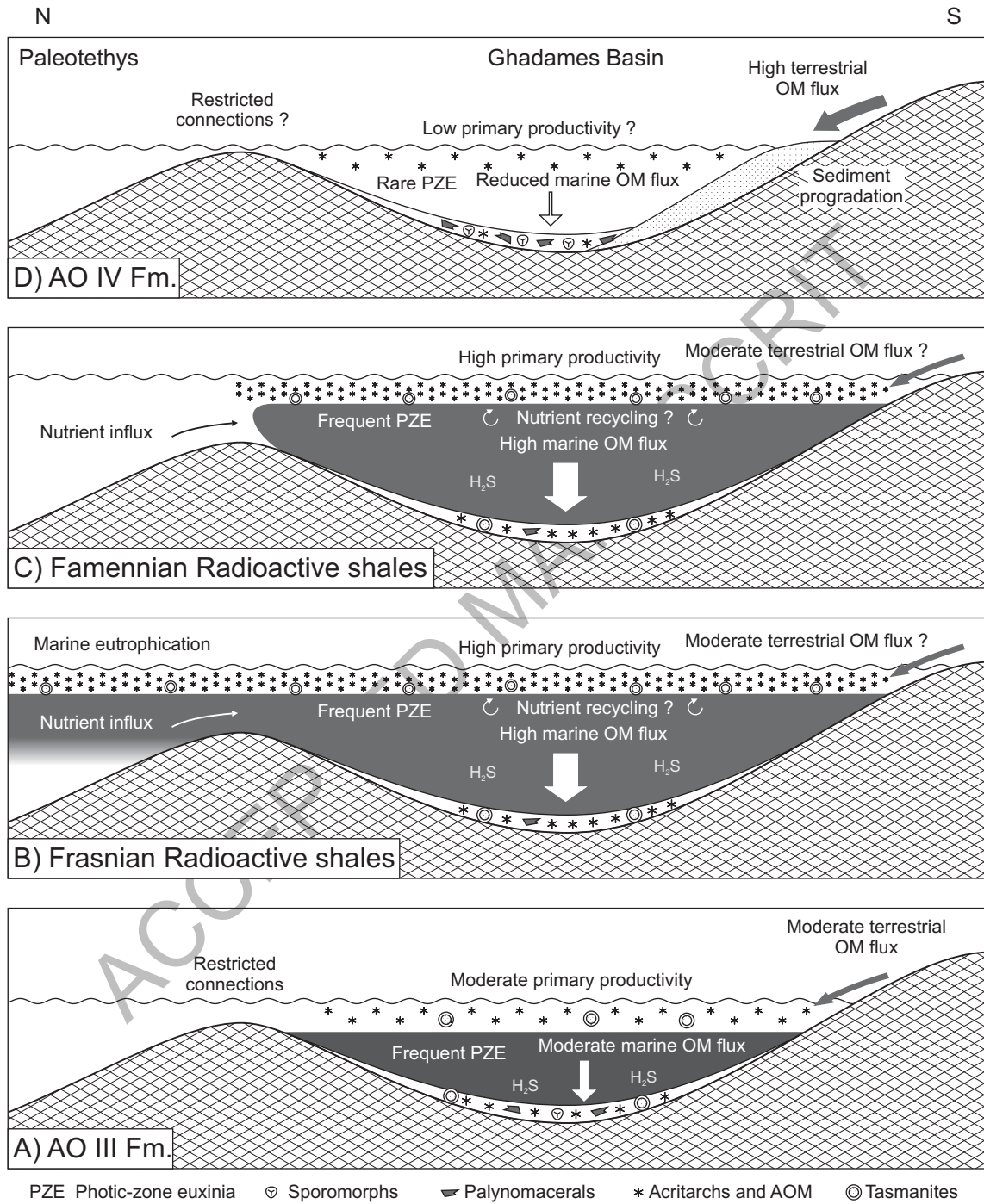


Figure 11

Tables

Table 1: Rock Eval and elemental analysis results of the samples from borehole D1-26.

Sample	S1 ¹	S2 ¹	Tmax °C	TOC %	PI ²	HI ³	OI ⁴	C _{min} (%)	S (%)	N (%)	TOC/N
7081	0.19	1.08	432	1.8	0.15	60	0	0.1	7.23	0.06	35
7083	0.24	1.78	434	2.68	0.12	66	0	0.14	3.73	0.08	39
7085	0.36	3.53	436	2.78	0.09	127	8	0.12	1.79	0.08	41
7087	0.15	1.01	439	0.86	0.13	117	48	0.96	1.27	0.03	33
7100	0.2	1.76	438	1.87	0.1	94	22	0.86	1.63	0.05	44
7712	0.85	2.8	434	2.21	0.23	127	5	0.16	3.23	0.12	21
7780	1.55	8.7	442	2.73	0.15	319	2	0.14	0.73	0.13	25
7800	0.7	0.77	431	1.06	0.48	73	27	0.13	2.55	0.07	18
7809	0.65	1.19	435	1.06	0.35	112	0	0.05	2.32	0.09	14
7810	0.78	2.2	441	1.29	0.26	171	12	0.09	1.95	0.1	15
7812	0.86	2.05	441	1.26	0.29	163	0	0.1	2.33	0.09	16
7813	0.73	2.2	440	1.38	0.25	159	4	0.12	2.17	0.08	20

¹ mgHC/g

² Production index: $PI = S1 / (S1 + S2)$

³ Hydrogen index in mgHC/gTOC

⁴ Oxygen index in mgCO₂/gTOC

Table 2: Biomarker ratios in the extracts of samples from borehole D1-26.

Sample	7085	7087	7712	7780	7810	7812
Source/environment						
Pr/Ph	2.07	2.23	1.29	1.01	1.30	1.42
Pr/C ₁₇	0.82	1.03	0.65	0.76	0.77	0.74
Ph/C ₁₈	0.43	0.53	0.51	0.69	0.66	0.57
CPI ¹	1.19	1.22	0.97	1.05	1.07	0.93
TAR ²	0.96	0.41	0.07	0.39	0.2	0.52
tricyclic/17 α hopanes ³	0.11	0	0.43	0.3	0.5	0.46
Hop/ster ⁴	3.6	3.24	1.41	1.32	1.27	1.22
%C ₂₇ ⁵	26.6	27.8	34.6	30.9	22.5	23.6
%C ₂₈ ⁵	23.5	17.3	14.2	17.5	22.9	30.2
%C ₂₉ ⁵	49.9	54.9	51.2	51.6	54.6	46.2
AIR* ⁶	2.22	1.02	0.84	0.4	0.86	1.26
Maturity						
Diasterane S/(S+R) ⁷	0.58	0.59	0.55	0.59	0.6	0.62
Sterane C ₂₉ S/(S+R) ⁸	0.43	0.45	0.48	0.5	0.48	0.33
Sterane C ₂₉ $\beta\beta$ /($\beta\beta$ + $\alpha\alpha$) ⁹	0.34	0.41	0.61	0.61	0.66	0.67
Hopane C ₃₂ 22S/(22S+22R)	0.6	0.59	0.62	0.56	0.6	0.56
Hopane C ₃₀ $\beta\alpha$ /($\beta\alpha$ + $\alpha\beta$)	0.17	0.15	0	0.13	0.15	0.16
Ts/(Ts+Tm)	0.35	0.36	-	0.72	0.81	0.82
MPI ¹⁰	0.62	0.73	0.61	0.66	0.73	0.81
MPR ¹¹	1.36	1.48	0.81	0.88	0.96	0.94
Vitrinite reflectivity Rc ¹²	0.77	0.84	0.77	0.79	0.84	0.89

¹ *n*-Alkanes Carbon Preference Index:

$$CPI = \{ [(C_{25} + C_{27} + C_{29} + C_{31} + C_{33}) / (C_{26} + C_{28} + C_{30} + C_{32} + C_{34})] + [(C_{25} + C_{27} + C_{29} + C_{31} + C_{33}) / (C_{26} + C_{28} + C_{30} + C_{32} + C_{34})] \} / 2$$

(Bray and Evans, 1961).

² *n*-Alkanes Terrestrial to aquatic ratio: TAR = (C₂₇ + C₂₉ + C₃₁) / (C₁₅ + C₁₇ + C₁₉) (Bourbonniere and Meyers, 1996).

³ $\Sigma(C_{21}-C_{29})$ cheilantanes / $\Sigma(C_{29}-C_{35})$ $\alpha\beta$ hopanes

⁴ Calculated using the sum of dia- and regular steroids and the sum of all hopanoids (diahopanes, TS series, hopanes and moretanes).

⁵ Relative percentage of C₂₇, C₂₈ and C₂₉ regular steranes, determined on the $\alpha\alpha\alpha$ R isomers.

⁶ Modified arylisoprenoid ratio: AIR* = (C₁₃-C₁₇) / (C₁₈-C₂₂) arylisoprenoids using both the 2,3,6- and 3,4,5-trimethyl-aryl isoprenoids on m/z 133+134 fragmentogram.

⁷ Calculated using C₂₇ $\beta\alpha$ diasteranes.

⁸ Calculated using C₂₉ $\alpha\alpha$ steranes.

⁹ Calculated using C₂₉ R and S stereoisomers.

¹⁰ Methylphenanthrene index MPI = 1.5[3-MP+2-MP] / [P+9-MP+1-MP] (Radke and Welte, 1983).

¹¹ Methylphenanthrene ratio MPR = [2-MP] / [1-MP] (Radke et al., 1982).

¹² Rc = 0.6 * MPI + 0.4 (Radke and Welte, 1983)

ACCEPTED MANUSCRIPT